

Implications of sterile neutrinos for medium/long-baseline neutrino experiments and the determination of θ_{13} .

Bhubanjyoti Bhattacharya,¹ Arun M. Thalapillil,¹ and Carlos E. M. Wagner^{1, 1, 2, 3}

¹*Enrico Fermi Institute and Department of Physics,*

University of Chicago, 5620 South Ellis Avenue, Chicago, IL 60637.

²*KICP and Dept. of Physics, Univ. of Chicago, 5620 S. Ellis Ave., Chicago IL 60637.*

³*HEP Division, Argonne National Laboratory, 9700 Cass Ave., Argonne, IL 60439.*

(Dated: March 29, 2022)

We revisit some of the recent neutrino observations and anomalies in the context of sterile neutrinos. Among our aims is to understand more clearly some of the analytic implications of the current global neutrino fits from short baseline experiments. Of particular interest to us are the neutrino disappearance measurements from MINOS and the recent indications of a possibly non-vanishing angle, θ_{13} , from T2K, MINOS and Double-CHOOZ. Based on a general parametrization motivated in the presence of sterile neutrinos, the consistency of the MINOS disappearance data with additional sterile neutrinos is discussed. We also explore the implications of sterile neutrinos for the measurement of $|U_{\mu 3}|$ in this case. We then turn our attention to the study of $|U_{e 3}|$ extraction in electron neutrino disappearance and appearance measurements. In particular, we study the effects of some of the additional CP phases that appear when there are sterile neutrinos. We observe that the existence of sterile neutrinos may induce a significant modification of the θ_{13} angle in neutrino appearance experiments like T2K and MINOS, over and above the ambiguities and degeneracies that are already present in 3-neutrino parameter extractions. There are reactor experiments, for instance those measuring ν_e disappearance like Double-CHOOZ, Daya Bay and RENO, where this modification is less significant and therefore the extracted $|U_{e 3}|$ value when sterile neutrinos are present is close to the one that would be obtained in the 3-neutrino case. Based on our study, we also conclude that the results from T2K imply a 90% C.L. lower-bound on $|U_{e 3}|$, in the “3 + 2” neutrino case, which is still within the sensitivity of future reactor neutrino experiments like Daya Bay, and consistent with the one- σ range of $\sin^2 2\theta_{13}$ recently reported by the Double-CHOOZ experiment. Finally, we argue that for the recently determined best-fit parameters, the results in the “3 + 1” scenario would be very close to the medium/long baseline results obtained in the “3 + 2” case analyzed in this work.

Keywords: Neutrino oscillations, sterile neutrinos, long-baseline experiments, reactor angle.

I. INTRODUCTION

Neutrinos have now been unequivocally established to be massive particles, but with very small masses. Experiments over the past two decades have firmly established a framework of neutrino oscillations that describe solar, atmospheric and reactor neutrino experiments (see for instance [1] and references therein).

The experiments are consistent with the existence of three electroweak eigenstates (ν_e, ν_μ, ν_τ) and three mass-eigenstates (ν_1, ν_2, ν_3). While the absolute neutrino mass scale has been very difficult to measure, the mass squared differences between the mass-eigenstates ($\Delta m_{21}^2, \Delta m_{32}^2$) are known to good accuracy [1–3]. Also, two of the mixing angles in the lepton sector (θ_{12}, θ_{23}) are known to good significance [2–4] and the third (θ_{13}) is being measured and will be measured to better and better accuracy by current and forthcoming experiments [5–8]. It is already clear, for instance, that the mixing in the lepton sector is very distinct from the quark sector.

In spite of these spectacular successes there are still many outstanding questions related to neutrinos. For instance it is not understood why neutrinos have such tiny masses or why their mixing angles are so much different from the quark sector. There have also been discrepancies from various short-baseline experiments that have been very hard to accommodate in the three active-neutrino picture. This has led to many studies incorporating additional singlet neutrino states to the framework [9–13].

Our main focus in this paper will be to gain a better analytical understanding of scenarios with additional singlet neutrino states and how they may affect current and forthcoming medium/long-baseline neutrino experiments. We are particularly interested in the measurements from MINOS and the determination of the reactor angle θ_{13} at various medium/long-baseline neutrino experiments. A study similar in spirit to ours was done in [14], for the case of an additional sterile neutrino. The focus of our study will albeit be different from theirs and will also be motivated by the current global fits, incorporating two additional sterile neutrinos.

In sections II and III we briefly review the current state of neutrino experiments and the viability of sterile neutrinos in the context of the standard model and cosmology. In section IV we briefly outline the short-baseline limit of neutrino oscillations and the global fits based on them. We also fix our notations here. In section V we study the implications of

these short-baseline global fits to medium/long-baseline neutrino experiments and explore various theoretical features. In section VI we give a summary of our results.

II. CURRENT STATE OF NEUTRINO OBSERVATIONS

Let us briefly review the current state of neutrino parameters. In a three neutrino framework let us label the ν mass eigenstates by latin indices, $i \in (1, 2, 3)$, and electroweak eigenstates by greek indices, $\alpha \in (e, \mu, \tau)$.

In the three neutrino framework, various experiments have measured the two mass-squared differences to be [1–3]

$$\begin{aligned} |\Delta m_{32}^2| &\simeq 2.4 \times 10^{-3} \text{ eV}^2, \\ |\Delta m_{21}^2| &\simeq 7.6 \times 10^{-5} \text{ eV}^2. \end{aligned} \quad (1)$$

The overall mass-scale is not determined from oscillation experiments alone, but cosmological considerations imply [15, 16]

$$\sum_i m_{\nu_i} \lesssim 0.6 \text{ eV}. \quad (2)$$

This still leaves an ambiguity in the ordering of the mass eigenstates. If $\Delta m_{32}^2 > 0$ neutrinos are said to be in a *normal* mass hierarchy (NH) and if $\Delta m_{32}^2 < 0$ they are said to be in an *inverted* mass hierarchy (IH).

Similar to quarks and the CKM matrix, the electroweak and mass eigenstates in the lepton sector are related by a mixing matrix. The relevant angles in this Pontecorvo-Maki-Nakagawa-Sakata (PMNS) mixing matrix [17] are denoted by θ_{23} (related to atmospheric oscillations), θ_{13} (reactor oscillations), and θ_{12} (relevant to solar oscillations). They are currently measured to be in the intervals [1–8]

$$\begin{aligned} 37^\circ &\lesssim \theta_{23} \lesssim 56^\circ, \\ 0^\circ &\lesssim \theta_{13} \lesssim 13^\circ, \\ 30^\circ &\lesssim \theta_{12} \lesssim 38^\circ. \end{aligned} \quad (3)$$

There are very strong indications [3] that the atmospheric angle θ_{23} is close to maximal ($\pi/4$). Solar data [4] also favors a ‘Large Mixing Angle’ (LMA) solution that indicates large θ_{12} . These intervals roughly translate to a PMNS matrix of the form

$$\left| \mathcal{U}_{\text{PMNS}}^{\text{exp.}} \right| \sim \begin{pmatrix} 0.8 - 0.9 & 0.5 - 0.6 & 0 - 0.2 \\ 0.3 - 0.6 & 0.3 - 0.7 & 0.6 - 0.8 \\ 0.1 - 0.5 & 0.5 - 0.8 & 0.6 - 0.8 \end{pmatrix}. \quad (4)$$

Some comments are in order. The above matrix is very close to a *tribimaximal* mixing matrix which has vanishing θ_{13} and maximal θ_{12} , θ_{23} . The question of CP-violation in the lepton sector, even in the simplest case of neutrinos being Dirac particles, is at present open. This is intimately tied to the question of a vanishing θ_{13} , since in the event of a vanishing or extremely small value the relevant Jarlskog-invariant ($J_{\text{CP}} \sim \text{area of the unitarity triangle} \propto \sin 2\theta_{13}$) is also zero.

Though almost all the observations from atmospheric, reactor and solar neutrino experiments can be accommodated conveniently in a three active-neutrino framework, there are a few outliers that may suggest existence of additional *sterile* neutrinos (i.e. neutrinos that are electroweak singlets). Let us briefly review them.

LSND employed a liquid scintillation detector to search for $\bar{\nu}_\mu \rightarrow \bar{\nu}_e$ oscillations [18] with a baseline of about 30 m. The neutrino energies were such that $L/E \sim \mathcal{O}(1)$ (Km/GeV). An excess of about 88 events was observed in the $20 \text{ MeV} \lesssim E \lesssim 60 \text{ MeV}$ range. A conventional oscillation interpretation of the data requires $\Delta m^2 \sim 0.1 - 10 \text{ eV}^2$ and is referred to as the LSND anomaly [18].

MiniBooNE was designed to test the LSND anomaly. They searched for both $\nu_\mu \rightarrow \nu_e$ and $\bar{\nu}_\mu \rightarrow \bar{\nu}_e$ oscillations [19]. The E ($\sim 1 \text{ GeV}$) and L (745 m) were both much bigger than LSND, but L/E was still kept to be about the same. No oscillations in neutrino mode was observed above 475 MeV, but an unexplained 3σ excess of ν_e events was found below 475 MeV. Subsequently, a 2.8σ excess of $\bar{\nu}_e$ was observed in the range $475 \text{ MeV} \leq E \leq 1250 \text{ MeV}$ consistent with LSND. There are preliminary updates from the MiniBooNE collaboration for their anti-neutrino data [20] where there is an excess below 475 MeV similar to ν data, but the $\bar{\nu}_\mu \rightarrow \bar{\nu}_e$ signal above 475 MeV has now diminished from before [20].

Recently, a re-evaluation of the reactor anti-neutrino flux [21] also indicates a deficit from the expected value. The data sets used for the evaluation came from various experiments with very short baselines ($L < 100$ m). The observed to expected flux ratio was found to be 0.943 ± 0.023 compared to a previous value of 0.979 ± 0.029 .

There was also a puzzling discrepancy between muon neutrino and anti-neutrino disappearance data from the MINOS experiment [3, 22] where the best-fit for the $\bar{\nu}$ data exhibited a higher $\Delta\bar{m}^2$ and lower $\sin^2 2\bar{\theta}$ than the ν data. Since it is a survival probability being measured, a resolution of both ν and $\bar{\nu}$ data requires an effective CPT violation, say for instance through some non-standard matter interactions [25]. There is an updated measurement from the MINOS collaboration in the $\bar{\nu}$ mode giving $\Delta\bar{m}^2 < 3.37 \times 10^{-3} \text{ eV}^2$ at 90% C.L. assuming $\sin^2 2\bar{\theta} = 1.0$ [23]. The most current, preliminary best-fits give $|\Delta\bar{m}^2| = [2.62_{-0.28}^{+0.31}(\text{stat}) \pm 0.09(\text{syst.})] \times 10^{-3} \text{ eV}^2$, $\sin^2 2\bar{\theta} = 0.95_{-0.11}^{+0.10}(\text{stat.}) \pm 0.01(\text{syst.})$ for the new anti-neutrino data [23]. The previous discrepancy between ν and $\bar{\nu}$ data therefore seems to be almost resolved. Prior to these measurements by MINOS, the strongest constraints on $\bar{\nu}$ parameters were from a global fit dominated by Super-Kamiokande data that included both atmospheric ν_μ and $\bar{\nu}_\mu$ results [23, 24].

There have also been indications for a non vanishing θ_{13} from various experiments [26–28]. A non-zero θ_{13} has far-reaching implications for CP-violation in the lepton sector and the consistency of other neutrino parameter fits.

MINOS detected ν_e appearance at the far detector [26], compared to expected background, suggesting for $\delta_{\text{CP}} = 0$

$$\begin{aligned} 2 \sin^2 \theta_{23} \sin^2 2\theta_{13} &< 0.12 & (\text{NH}) , \\ 2 \sin^2 \theta_{23} \sin^2 2\theta_{13} &< 0.20 & (\text{IH}) . \end{aligned} \quad (5)$$

The best-fit points [26] for $2 \sin^2 \theta_{23} \sin^2 2\theta_{13}$ are deduced to be $0.041_{-0.031}^{+0.047}$ for normal (NH) and $0.079_{-0.053}^{+0.071}$ for inverted hierarchies (IH). $|\Delta m_{32}^2| = (2.32_{-0.08}^{+0.12}) \times 10^{-3} \text{ eV}^2$, $|\Delta m_{21}^2| = (7.59_{-0.21}^{+0.19}) \times 10^{-5} \text{ eV}^2$, $\theta_{23} = 0.785 \pm 0.001$ and $\theta_{12} = 0.60 \pm 0.02$ have been assumed in the above fits.

The T2K experiment [27] observed six ν_e events that pass all selection criteria at the far detector. This suggests, at 90% C.L., again for $\delta_{\text{CP}} = 0$

$$\begin{aligned} 0.03 &< \sin^2 2\theta_{13} < 0.28 & (\text{NH}) , \\ 0.04 &< \sin^2 2\theta_{13} < 0.34 & (\text{IH}) . \end{aligned} \quad (6)$$

The best-fit points [27] for $\sin^2(2\theta_{13})$ are found to be $0.11_{-0.06}^{+0.1}$ (NH) and $0.14_{-0.08}^{+0.11}$ (IH). The above T2K limits and best-fit values are extracted for $\sin^2 2\theta_{23} = 1.0$ and $\Delta m_{32}^2 = 2.4 \times 10^{-3} \text{ eV}^2$.

Most recently, there is a preliminary result [28] from Double-CHOOZ, based on the first 100 days of data, showing at 68% C.L.

$$\sin^2 2\theta_{13} = 0.085 \pm 0.029 (\text{stat.}) \pm 0.042 (\text{syst.}) . \quad (7)$$

This result is particularly interesting since, being a reactor neutrino disappearance measurement, it is independent of CP phases and the mass hierarchy.

Some of the above short-baseline discrepancies may be interpreted as being due to the presence of extra electro-weak singlet neutrinos. With this in mind, in the next section we briefly discuss the viability of sterile neutrinos.

III. STERILE NEUTRINOS

From the invisible Z-decay width and LEP measurements, the number of active-neutrino species is constrained to [1]

$$\begin{aligned} N_\nu^{\text{Z-width}} &= 2.92 \pm 0.05 , \\ N_\nu^{\text{LEP}} &= 2.984 \pm 0.008 . \end{aligned} \quad (8)$$

Also, as already mentioned, most of the current neutrino oscillation data can be accommodated in a three active-neutrino framework. The Troitzk [29] and Mainz [30] experiments give a mass bound of about

$$m_\nu < 2.3 \text{ eV} , \quad (9)$$

by measuring the endpoint region of the tritium β -decay spectrum. In cosmology, neutrinos play a significant role by effecting the expansion history and growth of primordial perturbations which lead to a tighter mass bound [15, 16]

$$m_\nu \lesssim 0.6 \text{ eV} , \quad (10)$$

for three flavor mixing. The KATRIN experiment [31] is speculated to reach a sensitivity of $m_\nu < 0.2 \text{ eV}$.

All these nevertheless still leave open the possibility of other neutrino species that are singlets under the SM gauge groups and therefore “sterile”. Trying to resolve the LSND and MiniBooNE anomaly with data from solar and atmospheric neutrino measurements require, as we noted in the last section, $\Delta m_{\text{sterile}}^2 \sim \mathcal{O}(1) \text{ eV}^2$. A similar mass squared difference is also required to reconcile the reactor anti-neutrino flux deficit. There are also some very controversial indications from the Heidelberg-Moscow experiment [32] of detecting a neutrino mass $0.17 \text{ eV} < m_{\beta\beta}$.

An analysis [33], a few years ago, combining data from cosmic microwave background (CMB), large scale structure (LSS) and Lyman- α constrained the mass of a fourth sterile neutrino to be $m_s < 0.23 \text{ eV}$ assuming they are thermal. In the non-thermal case it was shown that the constraints are non-trivial in the mass-density plane, but still viable. This was re-emphasized in a study [34] that combined the WMAP 7-year data, BBN, small-scale CMB observations and measurement of the Hubble parameter from the Hubble space telescope. The study concluded that the current data set mildly favors extra radiation in the universe and derived constraints on the number and mass of possible sterile neutrino species. More recently, in [35], the authors conclude that though sterile neutrinos are disfavored by hot dark matter limits in minimal ΛCDM , extending the standard cosmological framework to include additional relativistic degrees of freedom or a dark-energy equation of state parameter $w < -1$ can relax these constraints substantially.

Constraints were also put on active-sterile mixing by measuring neutral-current interactions at MINOS [36]. By measuring the depletion of the neutral current event rate at the far detector, a 90% limit was placed on the fraction of active neutrinos that transition to a sterile neutrino (assuming $\theta_{13}=0$) [36]

$$f_s = \frac{P_{\nu_\mu \rightarrow \nu_s}}{1 - P_{\nu_\mu \rightarrow \nu_\mu}} < 0.22 \text{ (0.40)} . \quad (11)$$

The number in the bracket is for the assumption $\theta_{13} = 11.5^\circ$ and $\delta_{CP} = \pi$.

Apart from experiments reviewed in the last section, we should also mention two other experiments - SAGE [37] and GALLEX [38]. They give for ν_e disappearance a measured to calculated ratio $R = 0.86 \pm 0.05$ consistent with each other. If interpreted as due to an additional sterile state, this corresponds to a $\Delta m_{\text{sterile}}^2 = 2.24 \text{ eV}^2$ and $\sin^2 2\theta_{ee} = 0.50$ [39]. This conclusion has been weakened though by a recent analysis [40], based on its consistency with KARMEN and LSND data.

Motivated by all these indications, extensive studies have been performed on fitting the short-baseline neutrino discrepancies to various models with sterile neutrinos and checking their consistency with other experiments [9–13].

The inclusion of additional sterile neutrinos to the three active ones adds more structure to the neutrino oscillation formalism, without changing the basic framework. “3 + s” refers to the case of 3 active and s sterile neutrinos. The case of 3 active neutrinos in the standard model shall henceforth be denoted as $3\nu\text{SM}$. For ‘n’ neutrinos (active and sterile) the total number of angles in the mixing matrix is $n(n-1)/2$. The angles that rotate sterile states to sterile states are not relevant for neutrino oscillations and hence this number can be trimmed to $3(n-2)$ angles. Similarly, the number of CP phases (Dirac) that could be present in the PMNS matrix is $(n-2)(n-1)/2$. The number of physical CP phases relevant to electroweak physics and oscillations is $2n-5$, after field re-definitions. For “3 + 1” this gives 6 angles, 3 phases and for “3 + 2” this gives 9 angles, 5 phases.

IV. NEUTRINO OSCILLATIONS AND THE SHORT-BASELINE LIMIT.

The probability for a neutrino state α oscillating into a state β in vacuum is given by

$$P(\nu_\alpha \rightarrow \nu_\beta) = \delta_{\alpha\beta} - 4 \sum_{i>j} \Re(U_{\alpha i}^* U_{\beta i} U_{\alpha j} U_{\beta j}^*) \sin^2(\Delta m_{ij}^2 \frac{L}{4E}) + 2 \sum_{i>j} \Im(U_{\alpha i}^* U_{\beta i} U_{\alpha j} U_{\beta j}^*) \sin(\Delta m_{ij}^2 \frac{L}{2E}) , \quad (12)$$

where i, j denote the mass eigenstates and α, β include both active and sterile neutrino eigenstates. \Re and \Im stand for the real and imaginary parts respectively. We will also use the notation $\Delta_{ij} = \Delta m_{ij}^2 L / 4E$.

In most oscillation experiments (which are constructed with sensitivity to a particular Δm^2) one can simplify the above by taking a two neutrino limit. In this limit we get the familiar result

$$P^{2\nu}(\nu_\alpha \rightarrow \nu_\beta) = \begin{cases} 1 - \sin^2 2\theta \sin^2(1.27 \Delta m^2 (\text{eV}^2) \frac{L(\text{Km})}{E(\text{GeV})}) & ; \alpha = \beta , \\ \sin^2 2\theta \sin^2(1.27 \Delta m^2 (\text{eV}^2) \frac{L(\text{Km})}{E(\text{GeV})}) & ; \alpha \neq \beta . \end{cases} \quad (13)$$

We note a few well known properties. In the two neutrino limit $P^{2\nu}(\nu_\alpha \rightarrow \nu_\beta; U_{eff}) = P^{2\nu}(\nu_\beta \rightarrow \nu_\alpha; U_{eff})$. In general $P(\nu_\alpha \rightarrow \nu_\beta; U) = P(\nu_\beta \rightarrow \nu_\alpha; U^*)$. Under the assumption of CPT, in addition to having the mass-squared differences same for both neutrinos and anti-neutrinos, we also have $P(\bar{\nu}_\alpha \rightarrow \bar{\nu}_\beta; U) = P(\nu_\beta \rightarrow \nu_\alpha; U)$. The above two results lead to the fact that $P(\bar{\nu}_\alpha \rightarrow \bar{\nu}_\beta; U) = P(\nu_\alpha \rightarrow \nu_\beta; U^*)$. Thus, note that it is the last term in Eq.(12)

Model	$\Delta m_{41}^2 (\text{eV}^2)$	$ U_{e4} $	$ U_{\mu 4} $	$\Delta m_{51}^2 (\text{eV}^2)$	$ U_{e5} $	$ U_{\mu 5} $	δ/π
“3 + 2”	0.47	0.128	0.165	0.87	0.138	0.148	1.64

TABLE I. Global best-fit points using SBL data for the “3 + 2” case [11].

that distinguishes neutrinos and anti-neutrinos (when the number of families is greater than 2) for $\alpha \neq \beta$, indicating CP violation (CPV).

It is also important to emphasize that for disappearance measurements or survival probability ($\alpha = \beta$) the last term vanishes. Hence, survival probabilities in vacuum will not be effected by any CP phases and must be the same for both neutrinos and anti-neutrinos if CPT holds. The last term being an odd-function of Δm^2 is also sensitive to the mass hierarchy of the neutrino species in principle.

We will be interested in two specific limits of Eq. (12). The first limit is the short-baseline (SBL) limit which is relevant approximately when $L \sim \mathcal{O}(1)$ Km, $E \sim \mathcal{O}(1)$ GeV and consequently $L/E \sim \mathcal{O}(1)$ (Km/GeV). The other limit we would be interested in is the long-baseline (LBL) limit where $L \gtrsim \mathcal{O}(10^2)$ Km and $L/E \gtrsim \mathcal{O}(10^2)$ (Km/GeV). An intermediate case where $L \sim \mathcal{O}(1)$ Km, $E \sim \mathcal{O}(10^{-3})$ GeV and $L/E \sim \mathcal{O}(10^3)$ (Km/GeV) is often called medium-baseline (MBL).

We are going to primarily focus on a “3 + 2” scenario as analyzed in the recent global fits [11], with additional mass squared differences in the $\mathcal{O}(1) \text{eV}^2$ range. The comprehensive global fits, to SBL neutrino experiments, in [11] use appearance data from LSND [18], MiniBooNE [19], KARMEN [41], NOMAD [42] along with disappearance data from Bugey [43], CHOOZ [5], Palo Verde [44] and CDHS [45]. The most recent analysis further includes full spectral data from SBL reactor experiments ROVNO [46], Krasnoyarsk [47], ILL [48] and Gösgen [49] through rate measurements as summarized in [21]. The main conclusion in the study is that the global fits to SBL oscillations, for a “3 + 2” case, improves significantly with the inclusion of the new reactor anti-neutrino flux data, though some tension remains in the overall fit [11]. The global-fit values of [11] from SBL experiments is shown in Table I. We will adopt these values to analyze MBL/LBL measurements. Rather than taking the numbers in Table I as numbers set-in-stone, our attitude rather will be to view them as quantifying, to good extent, potential effects of sterile neutrinos in SBL.

The SBL limit is the case most suitable for analyzing the LSND and MiniBoone experiments since they both were designed with a characteristic $L/E \sim 1$ (Km)/(GeV). A short-baseline (SBL) assumption leads to a simplification of the most general oscillation formula in Eq. (12). The following approximations may be made

$$\begin{aligned}\Delta m_{32}^2 &\rightarrow 0, \\ \Delta m_{21}^2 &\rightarrow 0,\end{aligned}\tag{14}$$

compared to Δm_{j1}^2 where $j > 3$. This is partly motivated by requirements from LSND and MiniBoone observations which require $\Delta m_{\text{sterile}}^2 \sim \mathcal{O}(1) \text{eV}^2$. If there were no sterile neutrinos with $\Delta m_{\text{sterile}}^2 \sim \mathcal{O}(1) \text{eV}^2$, then under the SBL approximation $P(\nu_\alpha \rightarrow \nu_\alpha; U) = 1$, as should be expected since the baseline is not sufficient for significant oscillations into other flavors.

Using the above assumptions in Eq. (12) we get for the “3 + 2” case

$$P_{\alpha\beta}(\text{CPV})_{\text{SBL}} = \delta_{\alpha\beta} - \sum_{i=4,5} 4\Re(\chi_{\alpha\beta}^i) \sin^2 \Delta_{i1} - 4\Re(\xi_{\alpha\beta}) \sin^2 \Delta_{54} + \sum_{i=4,5} 2\Im(\chi_{\alpha\beta}^i) \sin 2\Delta_{i1} + 2\Im(\xi_{\alpha\beta}) \sin 2\Delta_{54}, \tag{15}$$

where

$$\begin{aligned}\chi_{\alpha\beta}^i &= (\delta_{\alpha\beta} - U_{\alpha 4} U_{\beta 4}^* - U_{\alpha 5} U_{\beta 5}^*) (U_{\alpha i}^* U_{\beta i}), \\ \xi_{\alpha\beta} &= (U_{\alpha 5}^* U_{\beta 5} U_{\alpha 4} U_{\beta 4}^*).\end{aligned}\tag{16}$$

For $\alpha = \beta = e$ this gives,

$$\bar{P}(\bar{\nu}_e \rightarrow \bar{\nu}_e)_{\text{SBL}} = 1 - 4(1 - |U_{e4}|^2 - |U_{e5}|^2) \left[|U_{e4}|^2 \sin^2 \Delta_{41} + |U_{e5}|^2 \sin^2 \Delta_{51} \right] - 4|U_{e5}|^2 |U_{e4}|^2 \sin^2 \Delta_{54}. \tag{17}$$

When $\alpha \neq \beta$, the CP phase(s) can play a major role and the appearance or conversion probabilities may be different for neutrinos and anti-neutrinos. It may be shown that in the SBL approximation for “3 + 2” there is only one relevant phase [11]. Consider the case $\alpha = \mu$ and $\beta = e$. Define the relevant phase as (also see Appendix A)

$$\delta = \arg(U_{e4}^* U_{\mu 4} U_{e5} U_{\mu 5}^*). \tag{18}$$

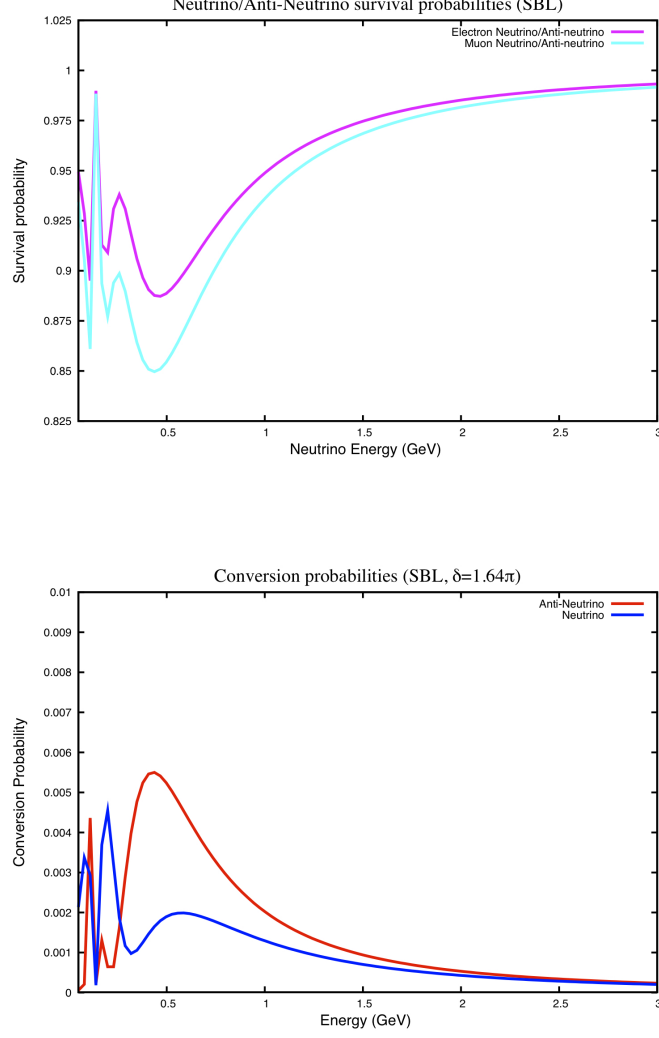


FIG. 1. Survival (P_{ee}) and conversion ($P_{\mu e}$) probabilities for neutrinos and anti-neutrinos in a SBL experiment with $L = 745$ m, assuming $\delta = 1.64\pi$ and parameters from Table I. The assumed distance to the detector corresponds to the baseline in MiniBooNE [19]. The difference in neutrino and anti-neutrino conversion probabilities is clearly visible in the bottom figure.

Then

$$\begin{aligned}
 \Re(\xi_{\mu e}) &= |U_{e4}^* U_{\mu 4} U_{e5} U_{\mu 5}^*| \cos \delta, & \Im(\xi_{\mu e}) &= |U_{e4}^* U_{\mu 4} U_{e5} U_{\mu 5}^*| \sin \delta, \\
 \Re(\chi_{\mu e}^4) &= -|U_{e4}|^2 |U_{\mu 4}|^2 - |U_{e4}^* U_{\mu 4} U_{e5} U_{\mu 5}^*| \cos \delta, & \Im(\chi_{\mu e}^4) &= |U_{e4}^* U_{\mu 4} U_{e5} U_{\mu 5}^*| \sin \delta, \\
 \Re(\chi_{\mu e}^5) &= -|U_{e5}|^2 |U_{\mu 5}|^2 - |U_{e4}^* U_{\mu 4} U_{e5} U_{\mu 5}^*| \cos \delta, & \Im(\chi_{\mu e}^5) &= -|U_{e4}^* U_{\mu 4} U_{e5} U_{\mu 5}^*| \sin \delta.
 \end{aligned} \tag{19}$$

As an aside, it should be mentioned that in the corresponding “3 + 1” case there is no CP phase that is relevant to the SBL limit and therefore the conversion probabilities in that case cannot distinguish between ν and $\bar{\nu}$, for instance, at MiniBooNE.

With the inclusion of a CP phase, from Eq. (15), we have for the conversion probabilities

$$P(\nu_\mu \rightarrow \nu_e; \text{CPV})_{\text{SBL}} = P(\nu_\mu \rightarrow \nu_e; \delta = 0)_{\text{SBL}} + 8|\xi_{\mu e}| \sin \Delta_{41} \sin \Delta_{51} \left[\cos(\Delta_{54} - \delta) - \cos \Delta_{54} \right], \tag{20}$$

$$\bar{P}(\bar{\nu}_\mu \rightarrow \bar{\nu}_e; \text{CPV})_{\text{SBL}} = P(\nu_\mu \rightarrow \nu_e; \delta = 0)_{\text{SBL}} + 8|\xi_{\mu e}| \sin \Delta_{41} \sin \Delta_{51} \left[\cos(\Delta_{54} + \delta) - \cos \Delta_{54} \right]. \tag{21}$$

To give a more holistic picture we plot the disappearance and appearance probabilities in Fig. 1, assuming MiniBooNE base length, with the matrix elements and CPV phase of Table I. We see that for low energies the depletion of ν_μ is greater than ν_e in the survival probability. Also note the expected enhancements and attenuations in the conversion probabilities, in this energy range, for $\bar{\nu}$ and ν . The presence of a non zero CP phase could therefore, in principle, explain the difference between ν and $\bar{\nu}$ measurements in MiniBooNE [50].

As we shall see, the effects of sterile states at the near detector (ND) will have implications also in LBL measurements since usually it is a ratio between the far detector (FD) and ND neutrino fluxes that are compared, to probe for oscillations. Thus a depletion of the neutrino flux at the ND due to sterile states will affect MBL/LBL measurements too.

V. LONG-BASELINE LIMIT OF NEUTRINO OSCILLATIONS.

We now turn our attention to LBL experiments and it is our intention to understand in more detail the consequences of the SBL fits, or equivalently the presence of the two sterile neutrino states, to these experiments. Specifically, we explore in this section the impact of the SBL global fits to MINOS disappearance measurements and the recent θ_{13} determinations. The questions we would like to address are whether MINOS disappearance data can constraint or discriminate in a definite way the “3 + 2” case from 3ν SM and if the recent indications of a significant, non-vanishing reactor angle θ_{13} are effected drastically by sterile neutrino states, if they exist.

In the LBL limit the assumption is that L/E may be anywhere in the range $10^2 - 10^4$ or higher. The larger values are more appropriate for atmospheric and solar oscillations. For very large Δm^2 , the oscillations get averaged out inside the detector and we may replace $\sin^2(\Delta m^2 \frac{L}{4E})$ by its expectation value $(1/2)$. Consequently, Δm_{41}^2 and Δm_{51}^2 are now averaged out since they are $\mathcal{O}(1) \text{ eV}^2$. Δm_{21}^2 may also be set to zero to first approximation. We will include this to be non-zero later, when discussing θ_{31} determination.

Calculating the oscillation probability from Eq. (12), in the above limit, for “3 + 2” gives

$$P_{\alpha\beta}(\text{CPV})_{\text{LBL}} = \delta_{\alpha\beta} - 2\Re(\chi_{\alpha\beta}) - 4\Re(\xi_{\alpha\beta}) \sin^2 \Delta_{54} - 4\Re(\zeta_{\alpha\beta}) \sin^2 \Delta_{32} + \Im(\chi_{\alpha\beta}) + 2\Im(\xi_{\alpha\beta}) \sin 2\Delta_{54} + 2\Im(\zeta_{\alpha\beta}) \sin 2\Delta_{32} , \quad (22)$$

where

$$\begin{aligned} \chi_{\alpha\beta} &= (\delta_{\alpha\beta} - U_{\alpha 4} U_{\beta 4}^* - U_{\alpha 5} U_{\beta 5}^*) \sum_{i=4,5} U_{\alpha i}^* U_{\beta i} = \sum_{i=4,5} \chi_{\alpha\beta}^i , \\ \xi_{\alpha\beta} &= U_{\alpha 5}^* U_{\beta 5} U_{\alpha 4} U_{\beta 4}^* , \\ \zeta_{\alpha\beta} &= (\delta_{\alpha\beta} - U_{\alpha 3} U_{\beta 3}^* - U_{\alpha 4} U_{\beta 4}^* - U_{\alpha 5} U_{\beta 5}^*) (U_{\alpha 3}^* U_{\beta 3}) . \end{aligned} \quad (23)$$

For a survival probability ($\alpha = \beta$) this may be re-written as

$$P_{\alpha\alpha}^{\text{LBL}} \simeq (1 - 2\Re[\chi_{\alpha\alpha}]) \left[1 - \frac{4\Re[\zeta_{\alpha\alpha}]}{1 - 2\Re[\chi_{\alpha\alpha}]} \sin^2 \Delta_{32} \right] . \quad (24)$$

Here we have neglected the term proportional to $|\xi_{\alpha\beta}|$ which tends to be negligible numerically, since it is quartic in the sterile neutrino matrix elements.

We observe from Eq. (24) that in the case of additional sterile states there is an effective *normalization* factor modifying the survival probability as well as a *modification* of the coefficient ($\sim \sin^2 2\theta$ in 3ν SM) of the energy dependent term. Thus, we conclude that the LBL survival probability $P_{\alpha\alpha}^{\text{LBL}}$ in the presence of sterile neutrinos is of a general form

$$P_{\alpha\alpha}^{\text{LBL}} \simeq \mathcal{N}_\alpha [1 - \sin^2 2\vartheta_\alpha^{\text{eff.}} \sin^2 \Delta_{32}] , \quad (25)$$

with

$$\begin{aligned} \mathcal{N}_\alpha &= 1 - 2\chi_{\alpha\alpha} , \\ \sin^2 2\vartheta_\alpha^{\text{eff.}} &= \frac{4\zeta_{\alpha\alpha}}{1 - 2\chi_{\alpha\alpha}} . \end{aligned} \quad (26)$$

The normalization factor (\mathcal{N}_α), in principle, may be extracted by looking at asymptotically large neutrino energies. The $\sin^2 2\vartheta_\alpha^{\text{eff.}}$ coefficient determines the dip of the first minima. The modification to $\sin^2 2\vartheta$, when there are sterile neutrinos, has two parts - a direct modification of $\zeta_{\alpha\alpha}$ and a further scaling of this quantity by \mathcal{N}_α . Observe that the

quantities appearing in the LBL limit, \mathcal{N}_α and the modifying terms in $\sin^2 2\vartheta_\alpha^{\text{eff}}$, are completely determined by SBL measurements through the matrix elements.

Using the global fit values from Table I, the various quantities that appear in the survival probability, Eq. (22), may be computed as (for an assumed $U_{e3} = 0.1$ and $U_{\mu 3} = 0.707$)

$$\begin{aligned}\chi_{ee} &= 0.0342 \quad (3\nu\text{SM} : 0) , \\ \chi_{\mu\mu} &= 0.0467 \quad (3\nu\text{SM} : 0) , \\ \zeta_{ee} &= 0.0095 \quad (3\nu\text{SM} : 0.0099) , \\ \zeta_{\mu\mu} &= 0.225 \quad (3\nu\text{SM} : 0.25) .\end{aligned}\tag{27}$$

The numbers in the brackets are the corresponding values in the $3\nu\text{SM}$ case. Using the above values we get

$$\begin{aligned}P_{ee}^{3+2} &= 0.932 [1 - 0.0408 \sin^2 \Delta_{32}] , \\ P_{\mu\mu}^{3+2} &= 0.907 [1 - 0.993 \sin^2 \Delta_{32}] ,\end{aligned}\tag{28}$$

which is relevant to any FD in an MBL/LBL experiment, for instance, the MINOS FD. For comparison, in the $3\nu\text{SM}$ the expressions corresponding to above would have been

$$\begin{aligned}P_{ee}^{3\nu\text{SM}} &= 1 - 0.0396 \sin^2 \Delta_{32} , \\ P_{\mu\mu}^{3\nu\text{SM}} &= 1 - \sin^2 \Delta_{32} .\end{aligned}\tag{29}$$

Compared to the $3\nu\text{SM}$ prediction the overall flux is reduced by about 7% for ν_e and by as large as 10% for ν_μ in Eq. (28). The effective angle is seen to be not modified significantly in the survival probability and may still, in principle, be extracted to yield a value that is close to the true value. We will come back to this point again while discussing $|U_{\mu 3}|$ and $|U_{e 3}|$ determination. From Eqs. (27) and (28) we note explicitly that the modification to $\sin^2 2\vartheta$, when there are sterile neutrinos, is due to a direct modification of $\zeta_{\alpha\alpha}$ and a further scaling of this quantity by \mathcal{N}_α .

It is also to be re-emphasized that when the sterile neutrino $\Delta m_{\text{sterile}}^2$ is large there will also generally be an effect in the ND, apart from the above effects in the FD, especially for low E . Since neutrino experiments usually compare a ratio of the fluxes at the FD and ND, taking into account geometric and other effects, modifications at the ND due to sterile states may also become relevant along with the FD effects. We will in fact see that for the values in Table I, the ND effects at MINOS are not completely negligible.

Although we specifically derived the expressions and numerical values for the “3+2” case, *a similar parametrization should be valid for any “3+s” scenario* with $\Delta m_{\text{sterile}}^2 \sim \mathcal{O}(1) \text{ eV}^2$. Note also that owing to Eq. (25) being a survival probability, any CP phases that may be present are completely irrelevant. This is particularly important since the CP phases that are relevant in LBL experiments may in general be mutually exclusive to the ones that are relevant in SBL experiments [11]. Thus, the above features must be applicable independently of CP phase structures in the LBL limit. The CP phases relevant to LBL may nevertheless become important in neutrino appearance measurements as we shall see.

A. Sterile neutrinos and the MINOS disappearance data.

We now turn our attention to the analysis of MINOS muon neutrino and anti-neutrino disappearance data [3, 22, 23]. It is interesting to ask if the MINOS disappearance data can discriminate or put constraints on scenarios with sterile neutrinos, specifically “3+2”, as motivated by the SBL global fits. The quantity of interest here is the ratio of the observed events at the MINOS far detector ($L_{\text{FD}}^{\text{MINOS}} = 734 \text{ Km}$, 4.2 Kt fiducial mass) to that expected at the far detector if there were no neutrino oscillations. The latter is extrapolated from the MINOS near detector ($L_{\text{ND}}^{\text{MINOS}} = 1.04 \text{ Km}$, 23.7 t fiducial mass) through a Monte-Carlo, taking into account geometric and pion kinematic effects [3, 22, 23].

Simple fits to the MINOS neutrino (7.25×10^{20} protons on target (POT)) and anti-neutrino (2.95×10^{20} POT) data [3, 22, 23] are shown in Fig. 2 with various parametrizations, motivated by Eq. (25). For the anti-neutrino analysis we have taken the new preliminary data [23].

The values for the fit parameters are shown in Table II along with their 1σ errors. In the first parametrization (Case I) both Δm^2 and $\sin^2 2\vartheta_\mu$ are floated, as in the analysis of the MINOS collaboration. A physical boundary on $\sin^2 2\vartheta$ is not imposed in the fit. In the second parametrization (Case II) Δm^2 and the normalization \mathcal{N}_μ are free parameters with $\sin^2 2\vartheta_\mu$ fixed at 1. The implicit motivation here is that, as we saw previously, the $\sin^2 2\vartheta_\mu$ coefficient is modified only minimally in disappearance measurements even when sterile neutrinos are present. In the final parametrization (Case III) we float \mathcal{N}_μ , $\sin^2 2\vartheta_\mu$ and Δm^2 . In this context, it is worth re-emphasizing that the MINOS data shown is actually the ratio of the FD and ND neutrino fluxes and there will be deviations from Eq. (25), especially at low energies for the values given in Table I, due to ND effects.

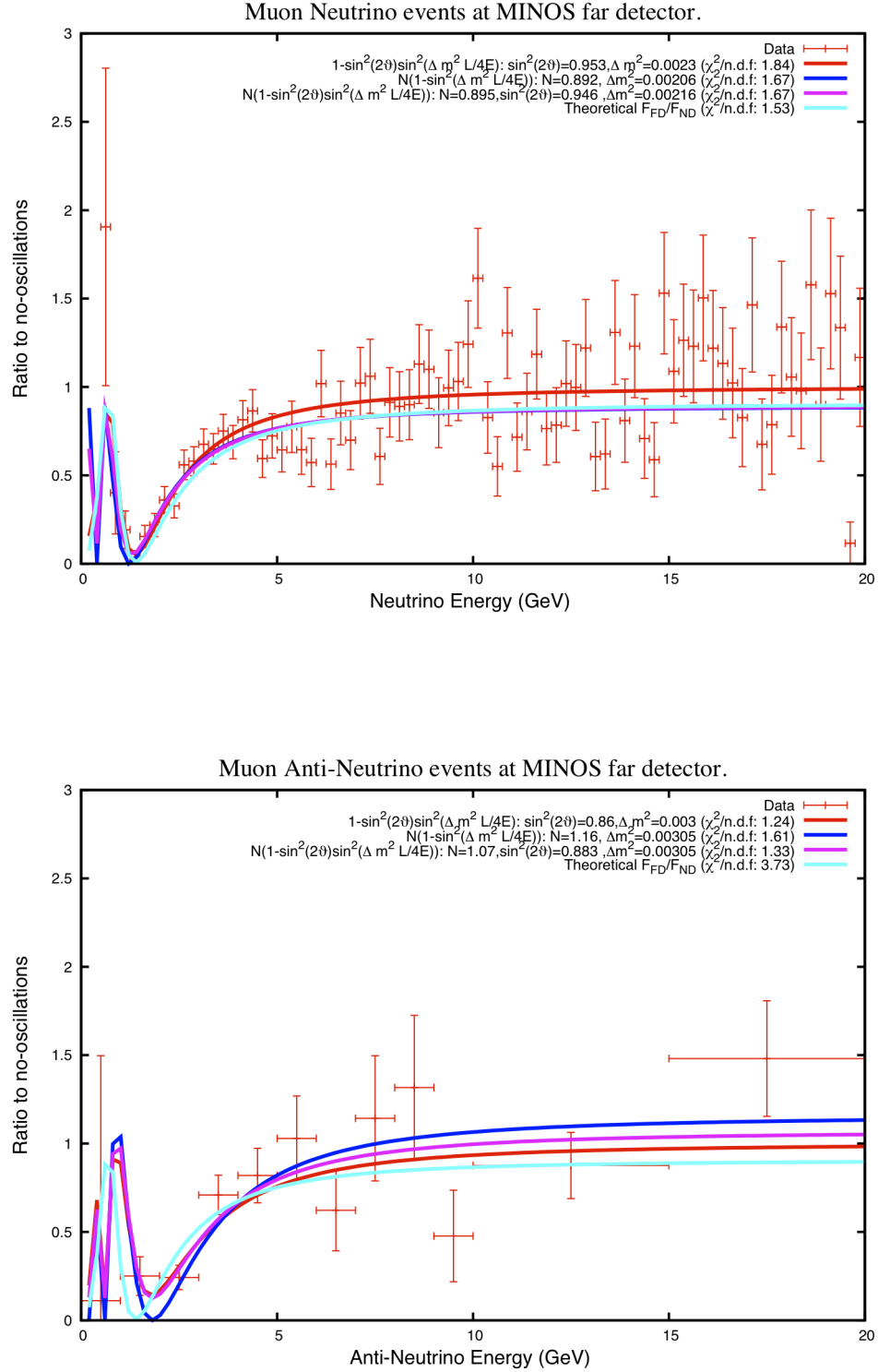


FIG. 2. Fits to MINOS neutrino [3] and anti-neutrino [22, 23] far-detector data assuming three different parametrizations motivated by Eq. (25) - Case I (red), Case II (dark blue) and Case III (purple). The theoretical curve from Eq. (30) (light blue), calculated based on the SBL global-fit values, is also shown. Though the plots are shown only till 20 GeV, the fits were done for the full range of neutrino energies in the data set (50 GeV for both ν_μ and $\bar{\nu}_\mu$). The neutrino data corresponds to 7.25×10^{20} POT and the anti-neutrino data to 2.95×10^{20} POT.

Case	$\Delta m^2 (10^{-3} \text{eV}^2)$	$\sin^2 2\vartheta_\mu$	\mathcal{N}_μ	$\chi^2/\text{n.d.f.}$
I	2.31 ± 0.10	0.953 ± 0.04	1^\dagger	1.65
II	2.07 ± 0.09	1^\dagger	0.895 ± 0.03	1.48
III	2.17 ± 0.13	0.946 ± 0.048	0.897 ± 0.03	1.48
$\mathcal{R}_{\mu\mu}$	—	—	—	1.53

Case	$\Delta \bar{m}^2 (10^{-3} \text{eV}^2)$	$\sin^2 2\bar{\vartheta}_\mu$	$\bar{\mathcal{N}}_\mu$	$\chi^2/\text{n.d.f.}$
I	3.0 ± 0.23	0.86 ± 0.08	1^\dagger	1.24
II	3.05 ± 0.2	1^\dagger	1.16 ± 0.13	1.61
III	3.05 ± 0.22	0.883 ± 0.086	1.07 ± 0.122	1.33
$\mathcal{R}_{\bar{\mu}\bar{\mu}}$	—	—	—	3.73

TABLE II. Parametric fits to MINOS neutrino and ant-neutrino data [3, 22, 23] for various parametrizations that take into account the possibility of sterile neutrinos, motivated by Eq. (25). The symbol \dagger denotes that the particular parameter is not floated in the fit under consideration.

The theoretical ratio of the flux at the FD and ND may be estimated from Eqs. (15) and (22) as

$$\mathcal{R}_{\mu\mu} = \frac{F_{\text{FD}}(\mu)}{F_{\text{ND}}(\mu)} \simeq \frac{1 - 2\chi_{\mu\mu} - 4\zeta_{\mu\mu} \sin^2(\Delta M_{32}^2 \frac{L_{\text{FD}}^{\text{MINOS}}}{4E})}{1 - \sum_{i>3} 4\chi_{\mu\mu}^i \sin^2(\Delta M_{i1}^2 \frac{L_{\text{ND}}^{\text{MINOS}}}{4E})}. \quad (30)$$

This ratio estimated from the SBL global-fit values is also plotted in Fig. 2. $|\Delta m_{32}^2| = 2.32 \times 10^{-3} \text{eV}^2$ has been assumed to calculate the theoretical curve. In the MINOS data set, the ND flux has been extrapolated to the FD, assuming no oscillations, including effects from beam-line geometry and meson decay kinematics [3, 22, 23]. $R_{\mu\mu}$ and $R_{\bar{\mu}\bar{\mu}}$, which are obtained assuming naively a collimated neutrino beam, may be directly compared to the real data sets to good approximation due to this. To quantify how the ratio predictions compare to the data sets, we may calculate a reduced- χ^2 ($\chi^2/\text{n.d.f.}$). It is found that the theoretical ratio prediction has a reduced- χ^2 of 1.53 and 3.73 for the neutrino and anti-neutrino data sets respectively (Table II).

From the neutrino data we extract an overall normalization, 0.897 ± 0.03 , that is close to the one theoretically calculated in Eq. (28) from the SBL global fits, which had a central value of 0.907. The extracted $\sin^2 2\vartheta_\mu$ (0.946 ± 0.048) is slightly lower than that predicted from the SBL global-fit values (0.993), but still within 1σ . The uncertainties are larger in the anti-neutrino data set and the number of data points is also smaller. For this case it is found that both the extracted normalization and $\sin^2 2\vartheta$ are significantly larger and smaller respectively than that predicted from SBL fits.

In Fig. 3 we plot the 68% and 90% likelihood contours for our simple fitting procedure, as applied to the MINOS neutrino data. Note that systematic uncertainties have not been taken into account as nuisance fit parameters. With the inclusion of a possible normalization \mathcal{N}_μ in the fits, the extracted Δm^2 decreases. The 90% C.L. lower bound on $\sin^2 2\vartheta$ also shifts marginally to a smaller value ($0.90 \rightarrow 0.886$) as we include \mathcal{N}_μ . Although we fix \mathcal{N}_μ in determining the 68% and 90% contours in Case III, the conclusions don't change significantly even if we include an error bar on \mathcal{N}_μ .

In the plots and fits shown, we have not changed the bin size from that given in the publicly available data set (the fits as done by the MINOS collaboration are for a bin size that is different from ours). We have nevertheless checked that re-binning the data (consistent with Fig. 2 of [3]) does not significantly change our observations. The MINOS collaboration also perform a more comprehensive likelihood analysis, compared to our fitting procedure, incorporating systematic uncertainties as nuisance parameters. For comparison, the values of the best-fits from the MINOS collaboration are $|\Delta m^2| = 2.32_{-0.08}^{+0.12} \times 10^{-3} \text{eV}^2$, $\sin^2 2\vartheta > 0.90$ (90% C.L.) for neutrinos [3] and $|\Delta \bar{m}^2| = [2.62_{-0.28}^{+0.31}(\text{stat}) \pm 0.09(\text{syst.})] \times 10^{-3} \text{eV}^2$, $\sin^2 2\bar{\vartheta} = 0.95_{-0.11}^{+0.10}(\text{stat.}) \pm 0.01(\text{syst.})$ for the new anti-neutrino data [22, 23]. So, although the central value is slightly different from ours, the lower bound on $\sin^2 2\vartheta$ is very close to the one obtained in our fit. The comparison between the $3\nu\text{SM}$ and “3 + 2” cases shows only a small shift of this lower bound and we expect this to be the case even after systematic errors are included.

Let us now try to derive some simple scaling relations between the $3\nu\text{SM}$ and “3 + 2” confidence intervals. In general, from Eq. (24), it may be shown that if α is a *lower-bound* (say the 90% C.L. limit) on the coefficient of $\sin^2 \Delta_{32}$ in $P_{\mu\mu}$, the matrix element $|U_{\mu 3}|$ would be constrained as

$$|U_{\mu 3}|_{\text{app}}^2 \in \left[\frac{1 - \sqrt{1 - \alpha}}{2}, \frac{1 + \sqrt{1 - \alpha}}{2} \right], \quad (31)$$

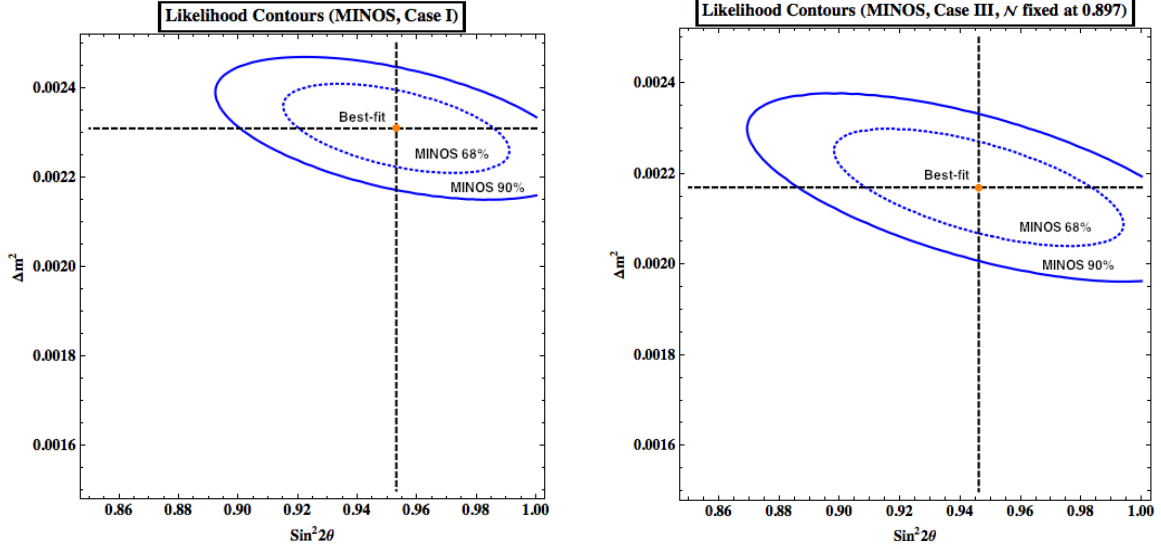


FIG. 3. Likelihood contours from our fitting procedure for MINOS neutrino data. The two plots are for Case I (left) and Case III (right) as defined in Table II. Systematic errors have not been included. It is observed that our 90% C.L. bound for $\sin^2 2\vartheta$ shifts slightly from 0.90 to 0.886, along with a reduction in Δm^2 , when we include a normalization factor \mathcal{N}_μ .

when the ‘incorrect’ assumption of 3ν SM and no sterile neutrinos is made. With the assumption as “3 + 2” we would have a constraint on the “true” value

$$|U_{\mu 3}|_{true}^2 \in \left[\frac{\beta'_\mu - \sqrt{\beta'^2_\mu - \mathcal{N}_\mu \alpha}}{2}, \frac{\beta'_\mu + \sqrt{\beta'^2_\mu - \mathcal{N}_\mu \alpha}}{2} \right], \quad (32)$$

where

$$\beta'_\mu = 1 - |U_{\mu 4}|^2 - |U_{\mu 5}|^2, \quad (33)$$

$$\mathcal{N}_\mu = 1 - 2\chi_{\mu\mu} = 1 - 2\beta'_\mu (1 - \beta'_\mu). \quad (34)$$

It is easy to see from the above equations that the *allowed interval for the extracted $|U_{\mu 3}|$ is shifted slightly, to lower values, when one includes sterile neutrinos in the extraction procedure.* Also note that in the case of the sterile-neutrinos, due to the modification, *the coefficient of $\sin^2 \Delta_{32}$ (which would have been $\sim \sin^2 2\theta_{23}$ in the 3ν SM case) can never be unity.*

For the $\sin^2 2\vartheta > 0.90$ (90% C.L.) 3ν SM (Case I) bound of Fig. 3 (left plot) this translates to

$$|U_{\mu 3}|_{app.}^2 \in [0.34, 0.66], \quad (35)$$

and for the or the $\sin^2 2\vartheta > 0.886$ (90% C.L.) “3 + 2” scenario (Case III), Fig. 3 (right plot), it becomes

$$|U_{\mu 3}|_{true}^2 \in [0.32, 0.63]. \quad (36)$$

The extracted $|U_{\mu 3}|$ indeed shifts downwards by a few percent from the 3ν SM case, when “3 + 2” is assumed. This will be relevant to us when we discuss ν_e appearance measurements, since the value assumed for $|U_{\mu 3}|$ will have a bearing on the extracted $|U_{e 3}|$ in that case.

It is clear from the analysis of the MINOS neutrino and anti-neutrino data sets that they by themselves cannot distinguish between the 3ν SM and “3 + 2” cases in a definite way. There nevertheless is a marginal improvement in the reduced- χ^2 , in the neutrino fits, when sterile neutrinos are included. The normalization as extracted from the neutrino data is close to that theoretically predicted for the FD and including any ND effects from sterile states improves the fit slightly. The uncertainties in the anti-neutrino data are larger and the reduced- χ^2 obtained for the theoretical prediction is poor. With higher statistics the analysis in the anti-neutrino sector may be improved in the future.

We will now explore the effects of sterile neutrinos on θ_{13} determination, in the context of ν_e disappearance and appearance measurements.

B. Effects of sterile neutrinos on the determination of θ_{13}

There have been recent indications from experiments like T2K, MINOS and Double-CHOOZ for a possibly non-zero θ_{13} . Let us try to understand the implications of sterile neutrinos for θ_{13} determination in these present and upcoming MBL/LBL experiments. If there are sterile neutrinos with $\Delta m_{\text{sterile}}^2 \sim \mathcal{O}(1) \text{ eV}^2$, then the mixing angles corresponding to them may be extracted in principle solely from SBL experiments. These matrix elements thus extracted, may then be used in the analysis of MBL/LBL experiments that aim to measure the reactor angle θ_{13} . Due to the presence of the additional sterile states there may be possible modifications to the extracted θ_{13} angle or more precisely the extracted matrix element $|U_{e3}|$.

1. Reactor ν_e disappearance measurements

Let us first consider neutrino/anti-neutrino disappearance experiments which measure survival probabilities. The CHOOZ [5] experiment and its successors Double-CHOOZ [6], Daya Bay [7] and RENO [8] are examples in this category. We take Double-CHOOZ as an example for purposes of our discussion. At Double-CHOOZ the FD is at 1050m and the ND is expected to be placed 400m from the reactor cores. For these base lengths and E ($\sim 3 \text{ MeV}$) we may use the MBL approximation at the FD.

We have for the $\nu_e/\bar{\nu}_e$ survival probability, at the FD

$$P_{\text{LBL}}^{ee} = 1 - 2(|U_{e4}|^2 + |U_{e5}|^2 - |U_{e4}|^4 - |U_{e5}|^4 - |U_{e4}U_{e5}|^2) - 4(|U_{e3}|^2(1 - |U_{e3}|^2) - (1 - \beta'_e)|U_{e3}|^2) \sin^2 \Delta_{31} \\ - 4(|U_{e2}|^2(1 - |U_{e2}|^2) - (1 - \beta'_e)|U_{e2}|^2) \sin^2 \Delta_{21} + 8|U_{e2}|^2|U_{e3}|^2 \sin \Delta_{21} \sin \Delta_{31} \cos \Delta_{32} , \quad (37)$$

where, as before

$$\beta'_e = 1 - |U_{e4}|^2 - |U_{e5}|^2 . \quad (38)$$

Note that we have now retained Δm_{21}^2 terms explicitly. Since this is a survival probability, any CP phase that may be present in the MBL/LBL limit is completely irrelevant and does not cause any ambiguities. This is not the case, as we shall see, when we consider conversion probabilities where the phases may play a significant role. For the Double-CHOOZ baseline and characteristic E ($\sim 3 \text{ MeV}$), the terms which are proportional to Δ_{21} and quartic in sterile-neutrino matrix elements may be dropped without incurring significant errors. This leads to the familiar expression

$$P_{\text{LBL}}^{ee} \simeq 1 - 2\chi_{ee} - 4\zeta_{ee} \sin^2 \Delta_{32} , \quad (39)$$

derived in Eq. (24) before. This may now be rewritten as

$$P_{\text{LBL}}^{ee} \simeq \mathcal{N}_e [1 - \sin^2 2\vartheta_e \sin^2 \Delta_{32}] , \quad (40)$$

where

$$\mathcal{N}_e = 1 - 2\chi_{ee} \simeq 1 - 2(1 - \beta'_e) , \\ \sin^2 2\vartheta_e = \frac{4\zeta_{ee}}{1 - 2\chi_{ee}} \simeq 4 \frac{|U_{e3}|^2(\beta'_e - |U_{e3}|^2)}{1 - 2(1 - \beta'_e)} . \quad (41)$$

Under the 3-neutrino assumption this survival probability may have been written as

$$P_{\text{LBL}}^{ee} \simeq 1 - 4|U_{e3}|_{\text{app.}}^2 (1 - |U_{e3}|_{\text{app.}}^2) \sin^2 \Delta_{32} . \quad (42)$$

From this we may associate an “apparent” value for the θ_{13} angle, through the relation

$$\sin^2 2\theta_{13}^{\text{app.}} = 4|U_{e3}|_{\text{app.}}^2 (1 - |U_{e3}|_{\text{app.}}^2) , \quad (43)$$

leading to the standard form for the $\nu_e \rightarrow \nu_e$ survival probability

$$P_{\text{LBL}}^{ee} \simeq 1 - \sin^2 2\theta_{13}^{\text{app.}} \sin^2 \Delta_{32} . \quad (44)$$

In general, if α' is an *upper-bound* on the coefficient of $\sin^2 \Delta_{32}$ in the survival probability P_{ee} , we have the constraint

$$|U_{e3}|_{\text{app.}}^2 \leq \frac{1 - \sqrt{1 - \alpha'}}{2} , \quad (45)$$

$ U_{e3} _{\text{app.}}$	$4 U_{e3} _{\text{app.}}^2(1 - U_{e3} _{\text{app.}}^2)$	$ U_{e3} $	$4 U_{e3} ^2(1 - U_{e3} ^2)$
0.224	0.19	0.219	0.183
0.198	0.15	0.194	0.145
0.168	0.11	0.165	0.106
0.133	0.07	0.131	0.067
0.087	0.03	0.085	0.029

TABLE III. Comparison of some representative apparent and true values of measured $|U_{e3}|$ and $4|U_{e3}|^2(1 - |U_{e3}|^2)$ in a *neutrino disappearance experiment*. A “3 + 2” scenario is assumed and the matrix elements for the estimate are taken from the SBL global fits.

for the apparent value when the “incorrect” assumption of no sterile neutrinos is made. With the correct assumption we would have a constraint on the true value (the \mathcal{N}_e factor cancels while taking the FD/ND ratio)

$$|U_{e3}|_{\text{true}}^2 \equiv |U_{e3}|^2 \leq \frac{\beta'_e - \sqrt{\beta'^2_e - \mathcal{N}_e \alpha'}}{2}. \quad (46)$$

Note that compared to the $|U_{\mu 3}|$ extraction case in Eq. (32), we have dropped a solution that is already ruled out.

In Table III we list for comparison, values of $|U_{e3}|$ and $4|U_{e3}|^2(1 - |U_{e3}|^2)$ determined in the neutrino disappearance case, using the $3\nu\text{SM}$ (“apparent”) and “3 + 2” (“true”) assumptions. The true values for $|U_{e3}|$ are found to be generally smaller than the apparent values, as is to be expected from Eq. (46). Nevertheless we observe that, due to the absence of CP phase ambiguities, negligible matter-effects and smallness of the sterile-neutrino matrix elements, the value of $|U_{e3}|$ extracted in reactor neutrino disappearance experiments are not modified significantly even when sterile neutrinos are present. Due to this, the extracted value of θ_{13} even under the incorrect assumptions is still close to the true value.

The above observations are especially pertinent in view of the recent preliminary result from Double-CHOOZ [28], suggesting

$$\sin^2 2\theta_{13}^{\text{D-CHOOZ}} = 0.085 \pm 0.029 (\text{stat.}) \pm 0.042 (\text{syst.}) . \quad (47)$$

Although Double-CHOOZ currently lacks a near detector, they normalize their measurement to the Bugey experimental data [43], which accounts for an approximate 0.945 suppression factor with respect to the expected one. The result is then fitted to the form $1 - \sin^2 2\theta_{13} \sin^2 \Delta_{32}$ to extract the value of $\sin^2 2\theta_{13}$. The difference between the normalization factor extracted from the Bugey experiment and the \mathcal{N}_e predicted in the “3 + 2” neutrino scenario is small compared to the systematic and statistical errors. We expect that this small difference, between the energy independent normalization factors, will not lead to any relevant variation of the extracted $\sin^2 2\theta$ value obtained from the fit.

Taking the central value above and assuming that there are two additional sterile states, characterized by the values in Table I, gives

$$\begin{aligned} |U_{e3}|_{\text{app.}}^{\text{D-CHOOZ}} &= 0.147, \quad 4|U_{e3}|_{\text{app.}}^2(1 - |U_{e3}|_{\text{app.}}^2)^{\text{D-CHOOZ}} = 0.085, \\ |U_{e3}|^{\text{D-CHOOZ}} &= 0.145, \quad 4|U_{e3}|^2(1 - |U_{e3}|^2)^{\text{D-CHOOZ}} = 0.082. \end{aligned} \quad (48)$$

As emphasized before, the difference between the extracted values in the 3-neutrino scenario and in the “3 + 2” scenario is very small compared to the current errors.

Now, consider a standard parametrization of the “3 + 2” PMNS matrix

$$\mathcal{U}_{\text{PMNS}}^{3+2} = \prod_{j>i, i=1}^3 \mathbb{R}_{ij}, \quad (49)$$

where the product is to be done from right to left and \mathbb{R}_{ij} is a complex or real rotation matrix in the ij -plane (see Appendix A). Let us generically denote by θ_s the small sterile angles (θ_{ij} , $j > 3$). Using this parametrization, it may be seen that the coefficient in Eq. (41) is still very close to $\sin^2 2\theta_{13}$, the deviations being of $\mathcal{O}(\theta_s^4)$ (Appendix A). The quantity $|U_{e3}|$ is nothing but $\sin \theta_{13}$ in the $3\nu\text{SM}$ case. In the “3 + 2” case, using the standard parametrization, it gets modified to $\cos \theta_{14} \cos \theta_{15} \sin \theta_{13}$ (see Appendix A). The quantity $4|U_{e3}|^2(1 - |U_{e3}|^2)$ in the $3\nu\text{SM}$ case would have corresponded exactly to $\sin^2 2\theta_{13}$. In the “3 + 2” case it deviates from $\sin^2 2\theta_{13}$ by terms of $\mathcal{O}(\theta_s^2)$ (Appendix A). Note also that $J_{\text{CP}} \propto \sin 2\theta_{13}$ in the $3\nu\text{SM}$ case.

All the above conclusions are also applicable to upcoming experiments like Daya Bay [7] and RENO [8] that aim to measure θ_{13} through a disappearance measurement. This is to be contrasted with appearance measurements that we discuss next.

2. ν_e appearance measurements

The value of θ_{13} may also be deduced by looking for ν_e appearance in experiments that measure neutrino conversion probabilities. This includes experiments such as T2K [27] and MINOS [26].

Let us focus on T2K [27] for the purposes of our discussion. At T2K the neutrino energy peaks around 0.6 GeV and the ND(s) and FD are at 280 m and 295 Km respectively. This ensures $\Delta_{32} \sim \pi/2$ at the FD when $E \sim 0.6$ GeV, giving an oscillation maximum. These base lengths also enable us to use all the approximations for LBL again at the FD.

The transition probability, keeping Δm_{21}^2 explicitly, may be written as

$$\begin{aligned} P_{\text{LBL}}^{\mu e} = & 4|U_{\mu 3}|^2|U_{e 3}|^2 \sin^2 \Delta_{31} + 4|U_{\mu 2}|^2|U_{e 2}|^2 \sin^2 \Delta_{21} + 8|U_{\mu 3}^*||U_{e 3}||U_{\mu 2}||U_{e 2}^*| \sin \Delta_{31} \sin \Delta_{21} \cos(\Delta_{32} - \delta_3) \\ & + 4|U_{\mu 3}||U_{e 3}||\beta''| \sin \Delta_{31} \sin(\Delta_{31} - \delta_1) + 4|U_{\mu 2}||U_{e 2}||\beta''| \sin \Delta_{21} \sin(\Delta_{21} - \delta_2) + 2(|U_{\mu 4}|^2|U_{e 4}|^2 + |U_{\mu 5}|^2|U_{e 5}|^2 \\ & + |U_{\mu 4}||U_{e 4}^*||U_{\mu 5}||U_{e 5}^*| \cos \delta) \quad , \end{aligned} \quad (50)$$

where

$$\begin{aligned} \beta'' &= \sum_{i \geq 4} U_{\mu i}^* U_{e i} \quad , \\ \delta_1 &= \arg(U_{\mu 3}^* U_{e 3} \beta'') \quad , \\ \delta_2 &= \arg(U_{\mu 2}^* U_{e 2} \beta'') \quad , \\ \delta_3 &= \arg(U_{\mu 3}^* U_{e 3} U_{\mu 2} U_{e 2}^*) \quad . \end{aligned} \quad (51)$$

The only approximation we have made in Eq. (50) is to average terms containing large sterile mass-squared differences. In contrast to the previous case there now appears non-trivial CP phases, as this is a conversion probability. Due to the presence of these phases there could be interesting interferences between the various terms and it's seen that one can no longer drop terms, as we did in the survival probability case, without significant errors.

These phases which appear in the LBL limit are in general independent of the phase δ extracted from the SBL global fits. Also note that when $\beta'' \neq 0$ the phase δ_3 is not independent and is given by $\delta_1 - \delta_2$. The effective CP phases δ_1 and δ_2 may be related to the ‘fundamental’ CP phases δ_{12} and δ_{13} in some particular parametrization of $\mathcal{U}_{\text{PMNS}}^{3+2}$ (Appendix A).

To get a better understanding of what the various terms in Eq. (50) mean, we briefly look at the corresponding expression in the $3\nu\text{SM}$ case. In the $3\nu\text{SM}$ the conversion probability has the well-known form

$$P_{\mu e}^{\text{LBL}} \simeq P_{\text{ATM.}}^{3\nu\text{SM}} + P_{\odot}^{3\nu\text{SM}} + 2\sqrt{P_{\odot}^{3\nu\text{SM}} P_{\text{ATM.}}^{3\nu\text{SM}}} \cos(\Delta_{32} - \delta_3) \quad , \quad (52)$$

with

$$\begin{aligned} P_{\text{ATM.}}^{3\nu\text{SM}} &\cong \sin^2 \theta_{23} \sin^2 2\theta_{13} \sin^2 \Delta_{31} \quad , \\ P_{\odot}^{3\nu\text{SM}} &\cong \cos^2 \theta_{23} \sin^2 2\theta_{12} \sin^2 \Delta_{21} \quad . \end{aligned} \quad (53)$$

The first and second terms in Eq. (52) are the atmospheric and solar oscillation contributions. The last term denotes an ‘interference’ between the atmospheric and solar oscillations with a relative phase shift δ_3 . Label this term $P_{\odot-\text{ATM.}}^{\text{INT.}-\delta_3}$ and in terms of the matrix elements it is

$$P_{\odot-\text{ATM.}}^{\text{INT.}-\delta_3} \equiv 8|U_{\mu 3}^*||U_{e 3}||U_{\mu 2}||U_{e 2}^*| \sin \Delta_{31} \sin \Delta_{21} \cos(\Delta_{32} - \delta_3) \quad . \quad (54)$$

If we define $\delta_{CP} = -\arg(U_{e 3})$, then for small $|U_{e 3}|$ values, δ_3 in the $3\nu\text{SM}$ is almost equal to $-\delta_{CP}$. The $P_{\odot}^{3\nu\text{SM}}$ term is $\mathcal{O}(\Delta_{21}^2)$ and small for most experiments we are interested in. The $P_{\odot-\text{ATM.}}^{\text{INT.}-\delta_3}$ term is potentially sensitive to the mass hierarchy. Under $+\Delta m_{32}^2 \rightarrow -\Delta m_{32}^2$ it picks up a negative sign and the argument $(|\Delta m_{32}^2| - \delta_3) \rightarrow (|\Delta m_{32}^2| + \delta_3)$.

For later comparison to “3+2”, in Fig. 4 we make some illustrative plots in the $3\nu\text{SM}$ case, assuming T2K baseline (295 Km). Note that in the $3\nu\text{SM}$ case

$$8|U_{\mu 3}|^2|U_{e 3}|^2 = 2 \sin^2 \theta_{23} \sin^2 2\theta_{13} \quad . \quad (55)$$

Plotting this combined quantity in Fig. 4 (top left) and later allows us to readily consider a non-maximal atmospheric sector in $|U_{e 3}|$ extraction. The CP phase δ_3 now is almost equal to $-\delta_{CP}$, for small $|U_{e 3}|$. Note from Fig. 4 (top right) that the difference between NH and IH can be more pronounced as we move away from $\Delta_{32} \sim \pi/2$. The bi-probability plot, bottom figure in Fig. 4, shows the probability orbits in the $(P_{\mu e}, \bar{P}_{\bar{\mu} \bar{e}})$ plane. The orbits are traced as we vary

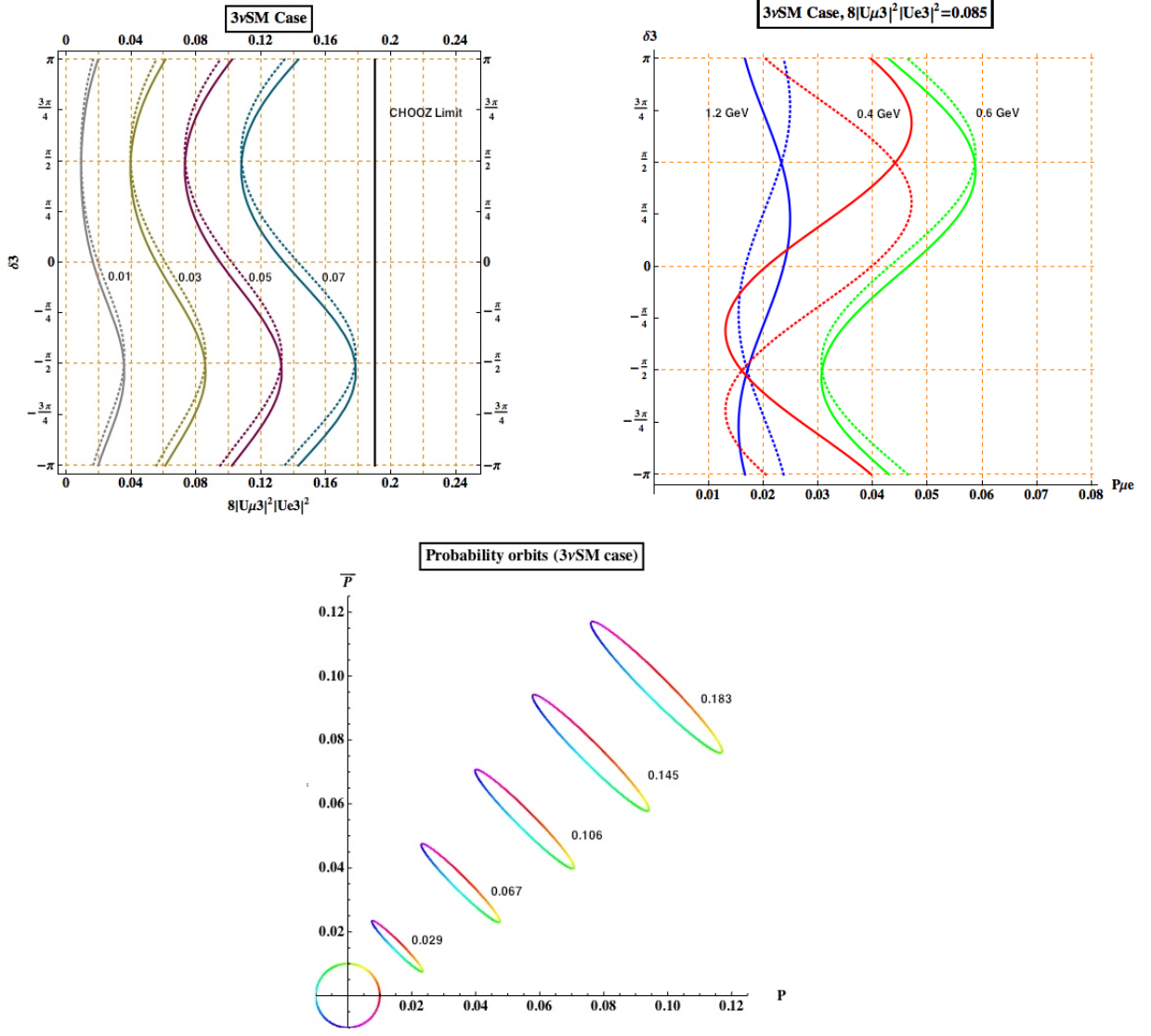


FIG. 4. Plots in the $3\nu\text{SM}$ case, assuming T2K baseline, showing extracted $8|U_{\mu 3}|^2|U_{e 3}|^2$ for $E = 0.6$ GeV (top-left plot) and conversion probabilities in the energy bins $\{0.4 \text{ GeV}, 0.6 \text{ GeV}, 1.2 \text{ GeV}\}$ for fixed $8|U_{\mu 3}|^2|U_{e 3}|^2$ (top-right plot). The thick-lines denote NH and the dotted lines denote IH. The top-left plot is for four fixed probabilities - 0.07, 0.05, 0.03 and 0.01. For comparison, the CHOOZ limit at 0.19 (90% C.L.) is shown. To avoid clutter, we have not shown in the plots the best-fit values from the other experiments - $0.041^{+0.047}_{-0.031}$ (MINOS-NH), $0.079^{+0.071}_{-0.053}$ (MINOS-IH), $0.11^{+0.1}_{-0.06}$ (T2K-NH), $0.14^{+0.11}_{-0.08}$ (T2K-IH) and 0.085 ± 0.051 (Double-CHOOZ preliminary) [26–28]. The bi-probability plot ($\bar{P}_{\mu\bar{e}}$ vs. $P_{\mu e}$) for five different values of $4|U_{e 3}|^2(1 - |U_{e 3}|^2)$, corresponding to Table III, is also plotted for the NH case. The color coding on them denotes the values of δ_3 and the values may be ascertained from the color wheel displayed at the origin. Apart from $|U_{e 3}|$, for simplicity, wherever applicable all other matrix elements have been assumed to be close to their tribimaximal values.

δ_3 , whose values may be read off from the color wheel at the origin, and the size of the ellipses are determined by the magnitude of $|U_{e 3}|$. Since $\Delta_{32} \sim \pi/2$ the $\cos \delta_3$ contribution in the interference term is small and the ellipses get squeezed as $\Delta_{32} \rightarrow \pi/2$, tending towards a line [51]. Due to this there is no (δ_3, θ_{13}) degeneracy in the plotted orbits. In this case, if matter matter effects are small (at T2K, for instance, they are small to good approximation), CP-violation can in principle be measured directly by comparing $P_{\mu e}$ and $\bar{P}_{\mu\bar{e}}$.

The first three terms in Eq.(50) correspond to these terms above - atmospheric, solar and an interference term between them. The next two terms in Eq.(50) are *contributions solely from sterile neutrinos and modulate the $P_{\text{ATM.}}^{3\nu\text{SM}}$*

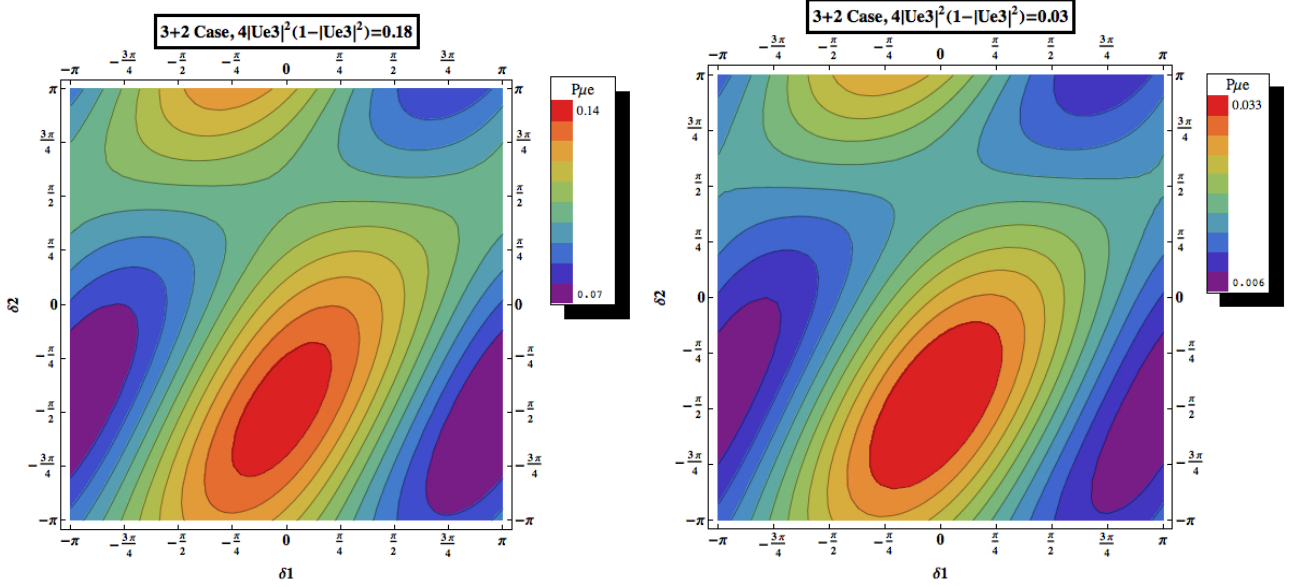


FIG. 5. Contour plots of $\nu_\mu \rightarrow \nu_e$ conversion probability, with T2K parameters, as a function of two independent phases δ_1 and δ_2 near $\Delta_{32} \sim \pi/2$ for the NH case. The color-coding denotes the magnitude of the conversion probability in each case. The quantity $4|U_{\mu 3}|^2(1 - |U_{\mu 3}|^2)$ in the 3ν SM case would have corresponded exactly to $\sin^2 2\theta_{13}$. In the “3 + 2” case, as we had commented earlier, it deviates from $\sin^2 2\theta_{13}$ by terms of $\mathcal{O}(\theta_s^2)$. In terms of $|U_{e3}|$ the above two plots correspond to 0.22 (left) and 0.085 (right), capturing the $|U_{e3}|$ range in Table III. In this case, besides $|U_{e3}|$ and the global-fit values of Table I, among all other matrix elements have been assumed to be close to their tribimaximal values.

and $P_{\odot}^{3\nu SM}$ with relative phase shifts of δ_1 and δ_2 respectively. Let us label these terms $\Delta P_{\text{ATM.}}^{\beta''-\delta_1}$ and $\Delta P_{\odot}^{\beta''-\delta_2}$,

$$\begin{aligned}\Delta P_{\text{ATM.}}^{\beta''-\delta_1} &\equiv 4|U_{\mu 3}||U_{e3}||\beta''| \sin \Delta_{31} \sin(\Delta_{31} - \delta_1), \\ \Delta P_{\odot}^{\beta''-\delta_2} &\equiv 4|U_{\mu 2}||U_{e2}||\beta''| \sin \Delta_{21} \sin(\Delta_{21} - \delta_2).\end{aligned}\quad (56)$$

The last three terms are energy independent residues obtained after averaging out terms involving large sterile neutrino mass-squared differences. Let us call these residue terms collectively as $\rho^{\text{res.}}$,

$$\rho^{\text{res.}} \equiv 2(|U_{\mu 4}|^2|U_{e4}|^2 + |U_{\mu 5}|^2|U_{e5}|^2 + |U_{\mu 4}||U_{e4}^*||U_{\mu 5}||U_{e5}| \cos \delta). \quad (57)$$

Though higher in order, they become important for small values of $|U_{e3}|$ to give a positive-definite conversion probability. It is also worth emphasizing that both $P_{\odot-\text{ATM.}}^{\text{INT.}-\delta_3}$ and $\Delta P_{\text{ATM.}}^{\beta''-\delta_1}$ are $\propto |U_{e3}|$. This observation will become relevant later when we try to understand cancellations among them.

In Fig. 5 we show contour plots of the conversion probability $P_{\mu e}$, for two fixed values of $|U_{e3}|$. T2K base length and characteristic neutrino energy have again been assumed. For the T2K ND distances (280 m) and $E_\nu = 0.6$ GeV, the effect of sterile neutrinos on the ND fluxes is minimal. Focusing primarily on $E_\nu \sim 0.6$ GeV may be justified by the fact that the J-PARC ν_μ beam has a very narrow side band [27] and in addition, under ideal conditions, most of the statistical power in $\sin^2 2\theta_{13}$ extraction may be expected to come from the region of the first oscillation maximum ($\Delta_{32} \sim \pi/2$), tuned at 0.6 GeV. We will look at the effects of varying E later for comparison.

Couple of things may be noted immediately from these contour plots in the (δ_1, δ_2) plane, at $\Delta_{32} \sim \pi/2$. The largest conversion to ν_e takes place in the vicinity of $(0, -\pi/2)$ in both cases. In fact this is found to be true for all intervening values of $|U_{e3}|$ as well. In this region both $P_{\odot-\text{ATM.}}^{\text{INT.}-\delta_3}$ and $\Delta P_{\text{ATM.}}^{\beta''-\delta_1}$ have the same sign and constructively interfere with $P_{\text{ATM.}}^{3\nu SM}$. Heuristically, let us denote this situation as

$$(0, -\pi/2) : P_{\mu e}^{\Delta_{32} \sim \pi/2} \sim P_{\text{ATM.}}^{3\nu SM} \oplus \left[P_{\odot-\text{ATM.}}^{\text{INT.}-\delta_3} \oplus \Delta P_{\text{ATM.}}^{\beta''-\delta_1} \right], \quad (58)$$

where \oplus denotes constructive interference and \ominus denotes destructive interference. As we decrease $|U_{e3}|$ the conversion probability decreases as expected but the maximal conversion region is relatively unchanged.

Similarly, the lowest conversion probabilities occur in the vicinity of $(\pm\pi, -\pi/2)$, where $P_{\odot-\text{ATM.}}^{\text{INT.}-\delta_3}$ and $\Delta P_{\text{ATM.}}^{\beta''-\delta_1}$ have the same sign but now destructively interfere with $P_{\text{ATM.}}^{3\nu\text{SM}}$,

$$(\pm\pi, -\pi/2) : P_{\mu e}^{\Delta_{32} \sim \pi/2} \sim P_{\text{ATM.}}^{3\nu\text{SM}} \ominus \left[P_{\odot-\text{ATM.}}^{\text{INT.}-\delta_3} \oplus \Delta P_{\text{ATM.}}^{\beta''-\delta_1} \right]. \quad (59)$$

Probably even more interesting is the observation of a thin band near $\delta_2 = \pi/2$ for which the conversion probability is almost constant over the full range of δ_1 . In this band there is an almost perfect cancellation between the $P_{\odot-\text{ATM.}}^{\text{INT.}-\delta_3}$ and $\Delta P_{\text{ATM.}}^{\beta''-\delta_1}$ terms,

$$(\forall\delta_1, +\pi/2) : P_{\mu e}^{\Delta_{32} \sim \pi/2} \sim P_{\text{ATM.}}^{3\nu\text{SM}} \oplus \left[P_{\odot-\text{ATM.}}^{\text{INT.}-\delta_3} \ominus \Delta P_{\text{ATM.}}^{\beta''-\delta_1} \right]. \quad (60)$$

The conversion probability in this case should almost be identical to the conversion probability in the $3\nu\text{SM}$ case, when the interference term $P_{\odot-\text{ATM.}}^{\text{INT.}-\delta_3}$ in the $3\nu\text{SM}$ limit almost completely vanishes (i.e. $(\Delta_{32} - \delta_3) \simeq \pm\pi/2$ in Eq. (52)). In the $3\nu\text{SM}$ case, near $\Delta_{32} \sim \pi/2$, this happens at $\delta_3 = 0$ and $\delta_3 = \pm\pi$. The conversion probabilities are indeed found to match as expected upon comparison. Again, for the global-fit and close-to-tribimaximal values we are working with, *this conclusion is seen to be true, independent of U_{e3} , since both $P_{\odot-\text{ATM.}}^{\text{INT.}-\delta_3}$ and $\Delta P_{\text{ATM.}}^{\beta''-\delta_1}$ are $\propto |U_{e3}|$.*

When $\delta_2 = 0$, it is seen that the terms $P_{\odot-\text{ATM.}}^{\text{INT.}-\delta_3}$ and $\Delta P_{\text{ATM.}}^{\beta''-\delta_1}$ are out of phase with each other by $\pi/2$ in the phase δ_1 (or now equivalently δ_3). Due to this, the conversion probability attains its maximum and minimum values at $\delta_3 = \pi/4$ and $\delta_3 = -3\pi/4$ respectively when $\Delta_{32} \sim \pi/2$.

In Fig. 6 we look at the probability orbits in the $(P_{\mu e}, \bar{P}_{\mu\bar{e}})$ plane for $\Delta_{32} \sim \pi/2$. We see a rich behavior in the orbits depending on the value of δ_2 . These may again be understood in terms of interference between $P_{\odot-\text{ATM.}}^{\text{INT.}-\delta_3}$ ($\bar{P}_{\odot-\text{ATM.}}^{\text{INT.}-\delta_3}$) and $\Delta P_{\text{ATM.}}^{\beta''-\delta_1}$ ($\Delta \bar{P}_{\text{ATM.}}^{\beta''-\delta_1}$), in $P_{\mu e}$ ($\bar{P}_{\mu\bar{e}}$). Since $P(\bar{\nu}_\alpha \rightarrow \bar{\nu}_\beta; U) = P(\nu_\alpha \rightarrow \nu_\beta; U^*)$, all the phases change sign as we go from neutrinos to anti-neutrinos. Specifically as seen from Eq. (60), for $\delta_2 = -\pi/2$, the $\bar{P}_{\odot-\text{ATM.}}^{\text{INT.}-\delta_3}$ and $\Delta \bar{P}_{\text{ATM.}}^{\beta''-\delta_1}$ terms cancel each other for $\bar{P}_{\mu\bar{e}}$ leaving a residue almost independent of δ_3 . This may be symbolically expressed as

$$(\forall\delta_1, -\pi/2) : \bar{P}_{\mu\bar{e}}^{\Delta_{32} \sim \pi/2} \sim P_{\text{ATM.}}^{3\nu\text{SM}} \oplus \left[\bar{P}_{\odot-\text{ATM.}}^{\text{INT.}-\delta_3} \ominus \Delta \bar{P}_{\text{ATM.}}^{\beta''-\delta_1} \right]. \quad (61)$$

It is also interesting to note that for $\delta_2 = 0$ the (δ_3, θ_{13}) degeneracy is reintroduced even when $\Delta_{32} \sim \pi/2$. This is clearly seen from the fact that the elliptic orbits for adjacent $|U_{e3}|$ values intersect. At the points of intersection both $\bar{P}_{\mu\bar{e}}$ and $P_{\mu e}$ have the same magnitudes for different values of δ_3 and $|U_{e3}|$. This degeneracy *can now mix CP-conserving and CP-violating solutions*. An example of this may be observed in the $\delta_2 = 0$ case of Fig. 6 where the orbit labelled by 0.183 intersects the orbit labelled by 0.106. The former solution is CP-violating ($\delta_3 \neq 0$) whereas the latter is CP-conserving ($\delta_3 \simeq 0$). Note that in the bi-probability discussions, to first approximation, the effects of the base length (L) and neutrino energy (E) only appear through $\Delta_{32} \sim \pi/2$. Due to this the general features of the probability orbits should be more widely valid, as long as we are in the vicinity of a conversion maximum.

Fig. 7 shows the extracted values of $8|U_{\mu 3}|^2|U_{e3}|^2$ for fixed conversion probabilities, again assuming that most of the statistical significance is coming from the region near $\Delta_{32} \sim \pi/2$. The thick-lines indicate NH and the dotted-lines indicate IH for comparison.

The different values of $8|U_{\mu 3}|^2|U_{e3}|^2$ extracted in Fig. 7 are easily understood by looking at the corresponding conversion probabilities near that particular CP phase region. For a fixed conversion probability, positive (negative) interference terms from $P_{\odot-\text{ATM.}}^{\text{INT.}-\delta_3}$ and $\Delta P_{\text{ATM.}}^{\beta''-\delta_1}$ must be compensated by lower (higher) value of $|U_{e3}|$. Therefore, the variation of the extracted $|U_{e3}|$ magnitude as we vary δ_3 must be anti-correlated with the conversion probability variation.

Another point we would like to emphasize is that the actual $|U_{e3}|$ value extracted depends on the assumed value of $|U_{\mu 3}|$, which may be extracted, as we saw in Eq. (32), from a ν_μ disappearance measurement such as MINOS. We saw in the case of LBL, and specifically MINOS, that the presence of sterile neutrinos cause the value of extracted $|U_{\mu 3}|$ also to shift to lower values by a few percent

$$|U_{\mu 3}|_{\text{extr.}}^{3+2} \lesssim |U_{\mu 3}|_{\text{extr.}}^{3\nu\text{SM}}. \quad (62)$$

Due to these considerations, plotting $8|U_{\mu 3}|^2|U_{e3}|^2$ in Fig. 7 allows us to incorporate a non-maximal atmospheric sector and $|U_{\mu 3}|$ readily. From Fig. 4 we observe that in the $3\nu\text{SM}$ case the extracted $|U_{e3}|$ is the same for normal and inverted hierarchy when $\delta_3 = \pm\pi/2 \forall E$. This is due to the fact that the interference term becomes $\propto \pm \sin^2 \Delta_{31}$ for $\delta_3 = \pm\pi/2$. It is also clear that the maximum difference between normal and inverted hierarchies occur at $\delta_3 = \{0, \pm\pi\} \forall E$, as expected from Eq. (52).

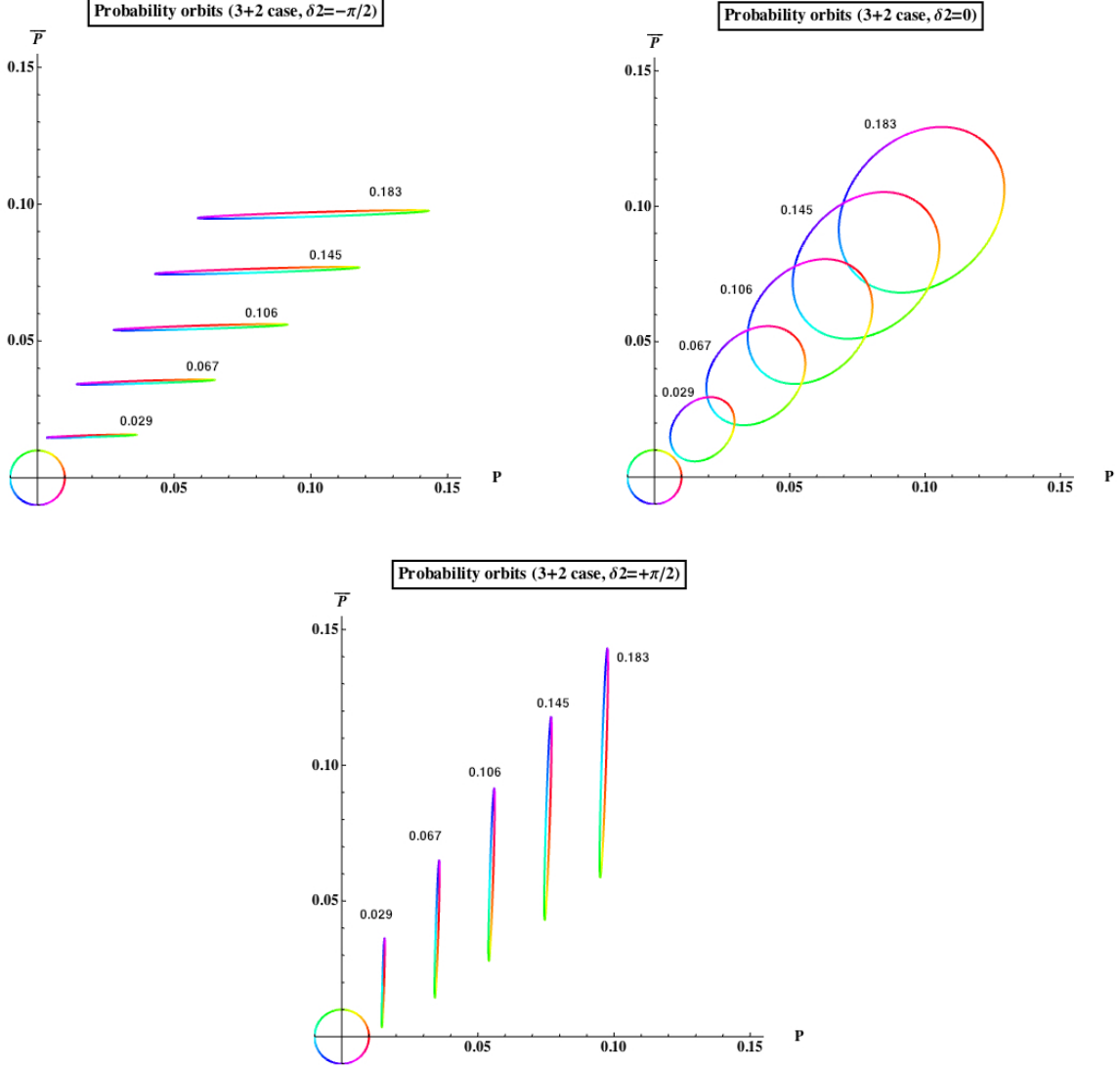


FIG. 6. Probability orbits in the “3 + 2” neutrino scenario for the NH case. The respective values of $4|U_{e3}|^2(1 - |U_{e3}|^2)$ are labelled on the orbits. As before, apart from $|U_{e3}|$ and the global-fits, all other matrix elements have been assumed to be close to their tribimaximal values. It is observed that in contrast to the 3ν SM case, the (δ_3, θ_{13}) degeneracy may be re-introduced depending on the value of the phase δ_2 . Also observe that $\delta_2 = -\pi/2$ and $\delta_2 = +\pi/2$ are orthogonal choices for which $\bar{P}_{\mu\bar{e}}$ and $P_{\mu e}$ remain almost constant respectively, as δ_3 traces the orbit. These may be compared to the 3ν SM probability orbits in Fig. 4. The value of δ_3 at any point in the orbit may again be deduced from the color wheel at the origin.

Along similar lines we can understand the behavior in the “3 + 2” case. The NH and IH cases should give the same extracted $|U_{e3}|$ when the terms which transform under $|\Delta m_{32}^2| \rightarrow -|\Delta m_{32}^2|$, specifically $P_{\odot-\text{ATM.}}^{\text{INT.}-\delta_3}$ and $\Delta P_{\text{ATM.}}^{\beta''-\delta_1}$, sum to the same numerical value, apart from the $|U_{e3}|$ factor that is common to both. If a term by term equivalence is demanded (which is a stronger condition than required) between NH and IH, we must have

$$\begin{aligned} [\cos(|\Delta_{32}| - \delta_3) + \cos(|\Delta_{32}| + \delta_3)] &\rightarrow 0, \\ [\sin(|\Delta_{31}| + \delta_1) - \sin(|\Delta_{31}| - \delta_1)] &\rightarrow 0, \end{aligned} \quad (63)$$

These give the solutions in the (δ_1, δ_2) space :

$$\text{NH} \equiv \text{IH} \quad \forall (L, E) : (0, \pm\pi/2), (\pi, \pm\pi/2), (-\pi, \pm\pi/2). \quad (64)$$

These regions are clearly visible in the top-left ($\delta_2 = -\pi/2$) and bottom ($\delta_2 = +\pi/2$) plots of Fig. 7, with the understanding that $\delta_3 = \delta_1 - \delta_2$.

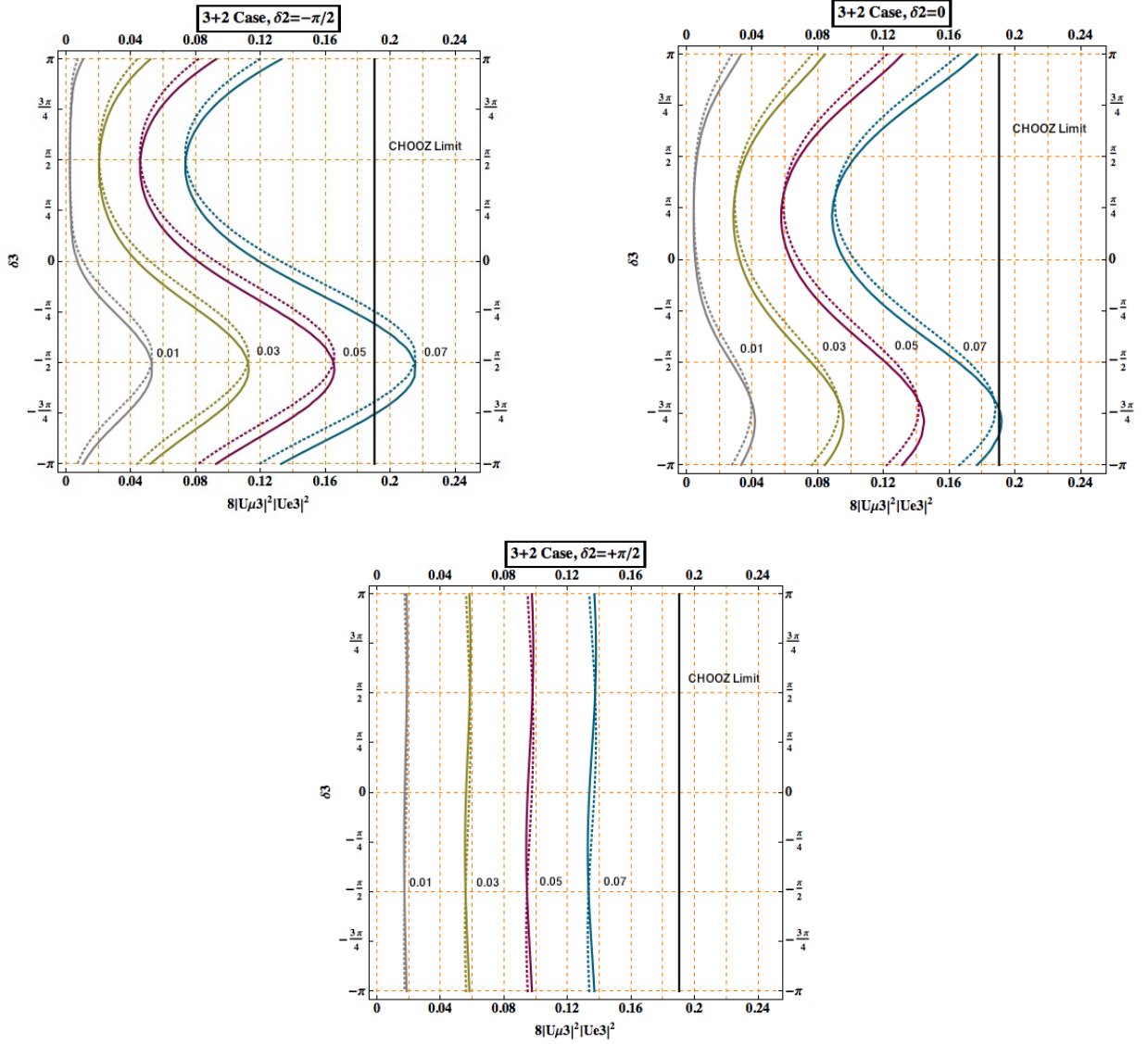


FIG. 7. Extracted values of $8|U_{\mu 3}|^2|U_{e 3}|^2$ in the “3 + 2” case, with T2K parameters ($L = 295$ Km, $E = 0.6$ GeV), assuming fixed conversion probabilities - 0.07, 0.05, 0.03, and 0.01. The thick-lines are for NH and the dotted-lines are for IH. We re-emphasize that the quantity $8|U_{\mu 3}|^2|U_{e 3}|^2$ plotted would exactly correspond to $2\sin^2\theta_{23}\sin^22\theta_{13}$ in the 3ν SM. The other matrix elements have been chosen as in the previous cases. For comparison, the preliminary best-fit value from Double-CHOOZ is at 0.085 ± 0.051 [28].

Imposing the weaker condition that the net sum of $P_{\odot-\text{ATM.}}^{\text{INT.}-\delta_3}$ and $\Delta P_{\text{ATM.}}^{\beta''-\delta_1}$ be equivalent in the NH and IH cases leads to the solution

$$\text{NH} \equiv \text{IH} \forall (L, E) : \frac{\sin \delta_1}{\cos(\delta_1 - \delta_2)} \simeq \frac{2|U_{\mu 2}||U_{e 2}^*| \sin \Delta_{21} \cos |\Delta_{32}|}{|\beta''| \cos |\Delta_{31}|}. \quad (65)$$

This is independent of $|U_{e 3}|$ and $|U_{\mu 3}|$. For $E = 0.6$ GeV ($\Delta_{32} \sim \pi/2$ for L_{T2K}), $(\delta_1, \delta_2) \sim (\pi/4, 0)$ and $(-3\pi/4, 0)$ are among the approximate solutions to the above equation. This equivalence between NH and IH can be seen clearly in the top-right plot of Fig. 7 near these regions.

For most of our theoretical discussions till this point, we were focused on the region near $\Delta_{32} \sim \pi/2$ at T2K, and hence at neutrino energies near 600 MeV. As perviously noted, it may be argued that this is not too egregious a choice since the J-PARC ν_μ beam has a very narrow side band and in addition, naively, most of the statistical power in $\sin^2 2\theta_{13}$ extraction must come from the region of the first oscillation maximum, tuned at 0.6 GeV. Nevertheless

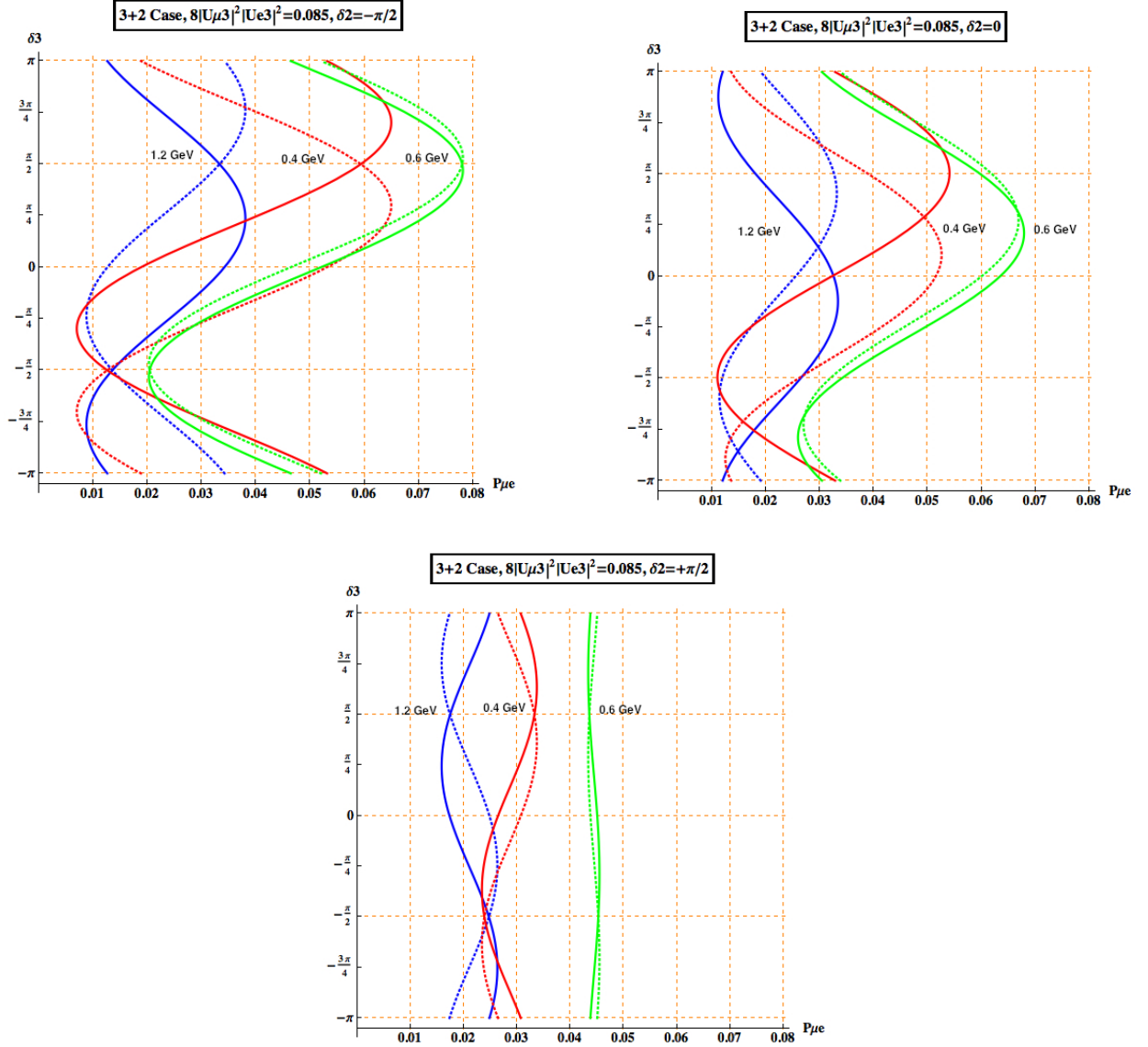


FIG. 8. Conversion probabilities $P_{\mu e}$ in the “3+2” case, for three different neutrino energies - 0.4 GeV (red), 0.6 GeV (green) and 1.2 GeV (blue). The thick-lines are for NH and the dotted-lines are for IH as before. They are plotted for a fixed $8|U_{\mu 3}|^2|U_{e 3}|^2$ of 0.085. It is clear that there may be significant differences between NH and IH depending on E and the CP phase structure.

it is important to explore the variations with E , especially considering that the T2K ν_e appearance measurement observed 4 events outside the 0.6 GeV bin.

Fig.8 shows the variation in the conversion probability $P_{\mu e}$ as we vary E for NH and IH. They are plotted for a fixed $8|U_{\mu 3}|^2|U_{e 3}|^2$ of 0.085. We focus on the 400 MeV, 600 MeV and 1200 MeV energy bins. These bins correspond to $\Delta_{32} \sim 3\pi/4$, $\Delta_{32} \sim \pi/2$ and $\Delta_{32} \sim \pi/4$ for the T2K baseline. As is clear, the variations may be substantial between NH and IH as we move away from the oscillation maximum depending on (δ_1, δ_2) . We could now pose the question - for a fixed conversion probability near $\Delta_{32} \sim \pi/2$ what is the smallest $|U_{e 3}|$ it may be associated with for any CP phase structure in the 3ν SM and “3 + 2” cases ?

In Fig. 9 we show the minimum attainable $|U_{e 3}|$ values, in terms of $4|U_{e 3}|^2(1 - |U_{e 3}|^2)$, in the 3ν SM and “3 + 2” scenarios. The range of conversion probabilities in Fig.9 correspond to those in Fig.7. Note that *the smallest possible $|U_{e 3}|$ in the “3 + 2” case is always significantly smaller than that possible in the 3ν SM,*

$$|U_{e 3}|_{\text{smallest}}^{3\nu\text{SM}} > |U_{e 3}|_{\text{smallest}}^{3+2} . \quad (66)$$

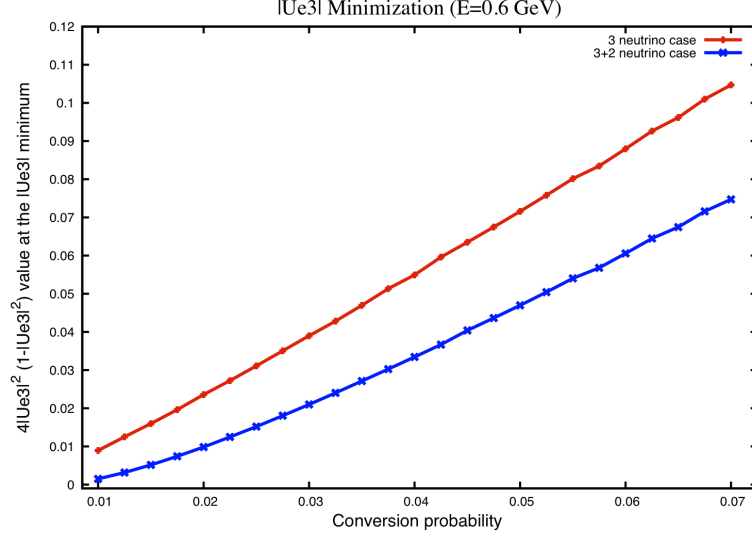


FIG. 9. Minimum possible $|U_{e3}|$ in the 3ν SM and “3 + 2” cases (NH and IH) expressed in terms of $4|U_{e3}|^2(1 - |U_{e3}|^2)$. In the plot, E is fixed at 0.6 GeV, the implicit assumption being that most of the statistical power in $|U_{e3}|$ extraction may come from the vicinity of $E \sim 0.6$ GeV (equivalently $\Delta_{32} \sim \pi/2$ for T2K baseline) which is the oscillation maximum. It is clear that the lower-bounds on the extracted $|U_{e3}|$ are generally much smaller with a “3 + 2” assumption, but still non-zero. The best-fit values in the 3ν SM for comparison are $-0.041^{+0.047}_{-0.031}$ (MINOS-NH), $0.079^{+0.071}_{-0.053}$ (MINOS-IH), $0.11^{+0.1}_{-0.06}$ (T2K-NH), $0.14^{+0.11}_{-0.08}$ (T2K-IH) and 0.085 ± 0.051 (Double-CHOOZ preliminary) [26–28].

Also observe that, though reduced, the smallest $|U_{e3}|$ values in “3 + 2” are still different from zero, albeit extremely tiny for small conversion probabilities. This is because, P_{\odot} and $\Delta P_{\odot}^{\beta''-\delta_2}$ by themselves are not sufficient to fulfill a given conversion probability in the range shown.

In the 3-neutrino scenario, from the T2K lower-bound curves [27] (which give the 90% C.L. lower bound on $\sin^2 2\theta_{13}$ as 0.03 – 0.04 for $\delta_{CP} = 0$), the smallest possible $\sin^2 2\theta_{13}$ is about 0.02 – 0.025, at $\delta_{CP} \simeq -\pi/2$. If we assume that the lower-bound curves correspond approximately to constant conversion probabilities, then using those approximate $P_{\mu e}$ values in the “3 + 2” scenario we may estimate, from Fig. 9, a lower limit for $4|U_{e3}|^2(1 - |U_{e3}|^2)$. This gives for the “3 + 2” case,

$$4|U_{e3}|^2(1 - |U_{e3}|^2) \gtrsim 0.008 - 0.01; \quad (|U_{e3}| \gtrsim 0.04 - 0.05) \quad \text{at 90\% C.L.} \quad (67)$$

Based on the above discussion, we note that in the “3 + 2” case, the results from T2K imply a 90% C.L. lower bound that is still within the reach (sensitivity) of future reactor neutrino experiments like Daya Bay [7], and consistent with the 1σ range of $\sin^2 2\theta_{13}$ recently reported by the Double-CHOOZ experiment.

3. Matter effects

All the above effects, due to the presence of sterile neutrinos, may be further modified by matter effects, depending on the base length and E . In the 3ν SM case these matter effects may be quantified as [52]

$$\begin{aligned} \mathcal{P}_{ee}^{3\nu\text{SM}} &= 1 - 4s_{13}^2 \frac{\sin^2(A_M - 1)\Delta_{31}}{(A_M - 1)^2} - \epsilon^2 \sin^2 2\theta_{12} \frac{\sin^2 A_M \Delta_{31}}{A_M^2}, \\ \mathcal{P}_{e\mu}^{3\nu\text{SM}} &= 4s_{13}^2 s_{23}^2 \frac{\sin^2(A_M - 1)\Delta_{31}}{(A_M - 1)^2} + 2\epsilon s_{13} \sin 2\theta_{12} \sin 2\theta_{23} \cos(\Delta_{31} - \delta_{CP}) \frac{\sin A_M \Delta_{31}}{A_M} \frac{\sin(A_M - 1)\Delta_{31}}{A_M - 1} \\ &\quad + \epsilon^2 \sin^2 2\theta_{12} c_{23}^2 \frac{\sin^2 A_M \Delta_{31}}{A_M^2}, \end{aligned} \quad (68)$$

where

$$\epsilon = \frac{\Delta m_{21}^2}{\Delta m_{31}^2} \quad , \quad A_M = \frac{2EV_M}{\Delta m_{31}^2} . \quad (69)$$

Eq. (68) is written to second order in ϵ and $\sin \theta_{13}$, assuming a constant matter-density potential [52]

$$V_M \simeq 7.56 \times 10^{-14} \left(\frac{\rho_{\text{crust}}}{\text{g/cm}^3} \right) Y_e \quad \text{eV} , \quad (70)$$

where ρ_{crust} is the crust matter density and Y_e is the number of electrons per nucleon. For earth matter $Y_e \simeq 0.5$ to very good approximation.

For a constant earth-crust density $\rho_{\text{crust}} \simeq 3 \text{ g/cm}^3$, we can estimate using the characteristic experimental parameters that

$$\begin{aligned} A_M^{\text{D-CHOOZ}} &\simeq 0.0003 , \\ A_M^{\text{T2K}} &\simeq 0.06 , \\ A_M^{\text{MINOS}} &\simeq 0.3 . \end{aligned} \quad (71)$$

Using the above values and Eq. (68) we can make estimates to convince ourselves that for Double-CHOOZ the matter effects are almost completely irrelevant and the extracted $|U_{e3}|$ is hardly affected. For T2K, it is seen that the matter effects are still relatively minimal (near $E \sim 0.6 \text{ GeV}$) but induce at most a few percent change in the extracted $|U_{e3}|$ relative to the vacuum assumption. In MINOS the matter effects can become more significant and may induce larger modifications of the extracted $|U_{e3}|$ somewhat obscuring any possible additional effects due to sterile neutrinos.

In both cases above, for a fixed conversion probability, the effect of matter interactions is to *decrease* (*increase*) the extracted $|U_{e3}|$ for NH (IH). This is probably most easily understood in a 2-neutrino limit by noting that the effect of the matter potential is to increase (decrease) the effective $\sin^2 2\theta_M$ coefficient for NH (IH). Crudely, to lowest order, the above conclusion should still hold approximately in the “3+2” neutrino case. Also note that in contrast to matter effects, the direction in which $|U_{e3}|$ was modified due to sterile neutrinos depended intricately on the (δ_1, δ_2) CP phase structure. A comprehensive analysis of θ_{13} extraction including matter-effects at MBL/LBL, in the presence of two sterile neutrinos, is beyond the scope of the present work (see [53] and references therein in this context, for a “3+1” SBL fit incorporating matter effects).

4. Comparison to the “3+1” case.

It is interesting to point out in the MBL/LBL limit that for $P_{\mu e}$, if one were to use the best-fit values in “3+1” for the matrix elements, as in [12] say, the numerical values of β'' and the energy independent residue term $\rho^{\text{res.}}$ defined in Eq. (57) comes out to be numerically almost the same. In the “3+2” case we have

$$\begin{aligned} |\beta''|_{\text{“3+2”}} &= 0.0351 , \\ \rho^{\text{res.}}_{\text{“3+2”}} &= 0.0021 \end{aligned} \quad (72)$$

and in the “3+1” case we get for the equivalent values,

$$\begin{aligned} |\beta''|_{\text{“3+1”}} &= 0.0354 , \\ \rho^{\text{res.}}_{\text{“3+1”}} &= 0.0025 . \end{aligned} \quad (73)$$

These quantities along with the 2 independent phases are the only relevant quantities in the LBL/MBL limit that depend on the presence of sterile neutrinos. The larger Δm_{41}^2 one obtains from SBL fits in “3+1”, relative to “3+2” Δm^2 values, is irrelevant for MBL/LBL since the terms containing it get averaged at the FD anyway.

VI. SUMMARY AND CONCLUSIONS

In the present study, we revisited some of the recent neutrino observations in the context of sterile neutrinos and the global fits from SBL experiments, to understand their impact on current and upcoming MBL/LBL measurements.

We noted that in general, for LBL experiments, the existence of sterile neutrinos lead to a distinct parametrization of the oscillation survival probabilities in terms of a normalization factor and a modified coefficient of the energy

dependent term. We analyzed the MINOS neutrino and anti-neutrino disappearance data [3, 22, 23] from this perspective. Though the parametrization does lead to a marginal improvement in fit, it was found that the current MINOS data by itself does not definitively discriminate the “3 + 2” scenario or the parameter values obtained from SBL fits. It was found that the $|U_{\mu 3}|$ confidence interval shifts to lower values by a few percent when the possible existence of sterile neutrinos are taken into account.

It was also commented that the recent measurements of a possibly non vanishing reactor angle θ_{13} may be affected by the existence of sterile neutrinos. We pointed out that the existence of sterile neutrinos may induce a modification of this angle (more precisely $|U_{e3}|$) in experiments that look at neutrino conversion probabilities, such as T2K and MINOS, and the perceived value may be shifted significantly from the “true” value in these cases. We also studied in detail the effects of additional sterile neutrino terms and their interference due to CP phases, in the “3 + 2” conversion probabilities. The probability orbits in the bi-probability plots also exhibited interesting features distinct from 3ν SM. It was, for instance, observed that the (δ_3, θ_{13}) degeneracy may be re-introduced depending on the CP phase structure in the “3 + 2” scenario and that there may be orbits where either the $\bar{P}_{\bar{\mu}\bar{e}}$ or $P_{\mu e}$ value remains almost constant with changing δ_3 .

It was also reiterated in the study that in the reactor experiments, these modifications due to sterile states are less significant. Due to this, the matrix element $|U_{e3}|$ when determined from survival probabilities under the 3ν SM assumption, is close to the “3 + 2” value, as compared to when determined from conversion probabilities. Neutrino disappearance experiments include Double-CHOOZ [6] and upcoming experiments such as Daya Bay [7] and RENO [8] that will measure θ_{13} to high precision. In this context we also conclude from our study that the results from T2K imply a 90% C.L. lower-bound on $|U_{e3}|$, in the “3 + 2” neutrino case, which is still within the sensitivity of future reactor neutrino experiments like Daya Bay [7], and consistent with the one- σ range of $\sin^2 2\theta_{13}$ recently reported by the Double-CHOOZ experiment. Finally, we argued that the results in the “3 + 1” scenario, using the recent best-fit values, would be very close to the medium/long baseline results we obtained in the “3 + 2” case. This was attributed to the numerical equivalence of the relevant parameters in both cases.

Our analysis suggests that if the SBL global fits, including the anomalies, are in fact legitimate indications of sterile neutrinos in nature, then there may be interesting effects in MBL/LBL neutrinos experiments. A more comprehensive study in the “3 + 2” scenario including matter effects at MBL/LBL terrestrial neutrino experiments, such as MINOS [26] and NuA [54], is left for future exploration. We also plan to pursue in future, a study of how the “3 + 2” scenario affects survival probabilities for solar neutrinos [55], using current global fit parameters.

ACKNOWLEDGMENTS

We thank E. Blucher, Z. Djurcic, J. Evans, G. O. Gann, M. Goodman, J. Kopp and M. Sanchez for discussions. C.W would like to acknowledge discussions with I. Mocioiu during an early investigation that partly motivated the present work. Work at ANL is supported in part by the U.S. Department of Energy (DOE), Div. of HEP, Contract DE-AC02-06CH11357. B.B and A.T were supported in part by the United States Department of Energy through Grant No. DE-FG02-90ER40560. A.T also acknowledges support from the Sidney Bloomenthal Fellowship during latter stages of this work.

Appendix A: Matrix elements

For completeness, we list some of the relevant matrix elements in terms of the angles and phases in a standard parametrization,

$$\mathcal{U}_{\text{PMNS}}^{3+2} = \prod_{j>i, i=1}^3 \mathbb{R}_{ij} . \quad (\text{A1})$$

The multiplication of matrices is to be performed from right to left. The rotation matrices may be real or complex. We choose a CP phase parametrization that is consistent with that employed in [11]. Under this convention the matrices \mathbb{R}_{12} , \mathbb{R}_{13} , \mathbb{R}_{15} , \mathbb{R}_{34} and \mathbb{R}_{35} carry CP phases.

The sterile neutrino matrix elements in this convention are

$$U_{e4} = \cos \theta_{15} \sin \theta_{14} , \quad (\text{A2})$$

$$U_{e5} = e^{-i\delta_{15}} \sin \theta_{15} , \quad (\text{A3})$$

$$U_{\mu 4} = \cos \theta_{14} \cos \theta_{25} \sin \theta_{24} - e^{i\delta_{15}} \sin \theta_{14} \sin \theta_{15} \sin \theta_{25} , \quad (\text{A4})$$

$$U_{\mu 5} = \cos \theta_{15} \sin \theta_{25} . \quad (\text{A5})$$

The sterile-neutrino angles ($\theta_{14}, \theta_{15}, \theta_{24}, \theta_{25}$) and phase δ_{15} can in principle be extracted from SBL measurements and specifically the global fits of Table I.

The active-neutrino matrix elements pertinent to our study come out to be

$$U_{e2} = \cos \theta_{13} \cos \theta_{14} \cos \theta_{15} e^{-i\delta_{12}} \sin \theta_{12} , \quad (\text{A6})$$

$$U_{e3} = \cos \theta_{14} \cos \theta_{15} e^{-i\delta_{13}} \sin \theta_{13} , \quad (\text{A7})$$

$$U_{\mu 2} = \cos \theta_{12} \cos \theta_{23} \cos \theta_{24} \cos \theta_{25} + e^{-i\delta_{12}} \sin \theta_{12} (\cos \theta_{13} (-\cos \theta_{25} \sin \theta_{14} \sin \theta_{24} - \cos \theta_{14} e^{i\delta_{15}} \sin \theta_{15} \sin \theta_{25}) \\ - \cos \theta_{24} \cos \theta_{25} e^{i\delta_{13}} \sin \theta_{13} \sin \theta_{23}) , \quad (\text{A8})$$

$$U_{\mu 3} = \cos \theta_{13} \cos \theta_{24} \cos \theta_{25} \sin \theta_{23} - e^{-i\delta_{13}} \sin \theta_{13} (\cos \theta_{25} \sin \theta_{14} \sin \theta_{24} + \cos \theta_{14} e^{i\delta_{15}} \sin \theta_{15} \sin \theta_{25}) . \quad (\text{A9})$$

The effective phases δ_1 and δ_2 can be related in principle to the ‘fundamental’ CP phases δ_{12} and δ_{13} using the above relations.

-
- [1] K. Nakamura *et al.* [Particle Data Group], J. Phys. G **37**, 075021 (2010).
 - [2] K. Abe *et al.* [Super-Kamiokande Collaboration], Phys. Rev. **D83**, 052010 (2011). [arXiv:1010.0118 [hep-ex]].
 - [3] P. Adamson *et al.* [MINOS Collaboration], Phys. Rev. Lett. **106**, 181801 (2011). [arXiv:1103.0340 [hep-ex]].
 - [4] B. Aharmim *et al.* (SNO), Phys. Rev. Lett. **101**, 111301 (2008).
 - [5] M. Apollonio *et al.* [CHOOZ Collaboration], Eur. Phys. J. **C27**, 331-374 (2003). [hep-ex/0301017].
 - [6] T. Akiri [Double Chooz Collaboration], Nucl. Phys. Proc. Suppl. **215**, 69-71 (2011).
 - [7] Z. Wang [Daya Bay Collaboration], [arXiv:1109.3253 [physics.ins-det]]; C. White [Daya Bay Collaboration], J. Phys. Conf. Ser. **136**, 022012 (2008).
 - [8] E. -J. Jeon [RENO Collaboration], Nucl. Phys. Proc. Suppl. **217**, 137-139 (2011).
 - [9] M. Sorel, J. M. Conrad, M. Shaevitz, Phys. Rev. **D70**, 073004 (2004). [hep-ph/0305255].
 - [10] A. E. Nelson, Phys. Rev. D **84**, 053001 (2011) [arXiv:1010.3970 [hep-ph]].
 - [11] J. Kopp, M. Maltoni, T. Schwetz, [arXiv:1103.4570 [hep-ph]]; M. Maltoni, T. Schwetz, Phys. Rev. **D76**, 093005 (2007). [arXiv:0705.0107 [hep-ph]].
 - [12] C. Giunti, [arXiv:1106.4479 [hep-ph]]; C. Giunti, M. Laveder, [arXiv:1107.1452 [hep-ph]].
 - [13] V. Barger, Y. Gao, D. Marfatia, [arXiv:1109.5748 [hep-ph]].
 - [14] A. de Gouvea, T. Wytock, Phys. Rev. **D79**, 073005 (2009). [arXiv:0809.5076 [hep-ph]].
 - [15] B. A. Reid, L. Verde, R. Jimenez, O. Mena, JCAP **1001**, 003 (2010). [arXiv:0910.0008 [astro-ph.CO]].
 - [16] M. C. Gonzalez-Garcia, M. Maltoni, J. Salvado, JHEP **1008**, 117 (2010). [arXiv:1006.3795 [hep-ph]].
 - [17] B. Pontecorvo, JETP **34**, 172 (1958); V. N. Gribov and B. Pontecorvo, Phys. Lett. B **28**, 493 (1969); Z. Maki, M. Nakagawa, and S. Sakata, Prog. Theor. Phys. **28**, 870 (1962).
 - [18] A. Aguilar *et al.* [LSND Collaboration], Phys. Rev. **D64**, 112007 (2001). [hep-ex/0104049].
 - [19] A. A. Aguilar-Arevalo *et al.* [The MiniBooNE Collaboration], Phys. Rev. Lett. **105**, 181801 (2010). [arXiv:1007.1150 [hep-ex]].
 - [20] E. Zimmerman [MiniBooNE Collaboration], PANIC 2011; Z. Djurcic [MiniBooNE Collaboration] NUFAC 2011; E. D. Zimmerman [MiniBooNE Collaboration], [arXiv:1111.1375 [hep-ex]].
 - [21] G. Mention, M. Fechner, T. Lasserre, T. A. Mueller, D. Lhuillier, M. Cribier, A. Letourneau, Phys. Rev. **D83**, 073006 (2011). [arXiv:1101.2755 [hep-ex]].
 - [22] P. Adamson *et al.* [MINOS Collaboration], Phys. Rev. Lett. **107**, 021801 (2011). [arXiv:1104.0344 [hep-ex]] .
 - [23] P. Adamson *et al.* [MINOS Collaboration], [arXiv:1108.1509 [hep-ex]]; See also the preliminary $\bar{\nu}$ data and plots at <http://www.numi.fnal.gov/PublicInfo/forscientists.html>.
 - [24] M. C. Gonzalez-Garcia and M. Maltoni, Phys. Rept. **460**, 1 (2008).
 - [25] L. Wolfenstein, Phys. Rev. D **17**, 2369 (1978); J. W. F. Valle, Phys. Lett. B **199**, 432 (1987); M. C. Gonzalez-Garcia *et al.*, Phys. Rev. Lett. **82**, 3202 (1999); A. Friedland, C. Lunardini, and M. Maltoni, Phys. Rev. D **70**, 111301 (2004).
 - [26] P. Adamson *et al.* [MINOS Collaboration], Phys. Rev. Lett. **107**, 181802 (2011). [arXiv:1108.0015 [hep-ex]].
 - [27] K. Abe *et al.* [T2K Collaboration], Phys. Rev. Lett. **107**, 041801 (2011). [arXiv:1106.2822 [hep-ex]].
 - [28] H. De Kerret [Double-CHOOZ Collaboration], LowNu 2011.
 - [29] V. N. Aseev, A. I. Belev, A. I. Berlev, E. V. Geraskin, A. A. Golubev, N. A. Likhovid, V. M. Lobashev, A. A. Nozik *et al.*, [arXiv:1108.5034 [hep-ex]]; V. M. Lobashev Progress in Particle and Nuclear Physics **48** (2002) pp. 123-131.
 - [30] Ch. Weinheimer, B. Degen, A. Bleile, J. Bonn, L. Bornschein, O. Kazachenko, A. Kovalik, E. W. Otten Phys. Lett. B **460** (1999) 219.
 - [31] G. Drexlin *et al.*, Nucl. Phys. B (Proc. Suppl.) **145** (2005) 263-267
 - [32] H. V. Klapdor-Kleingrothaus, I. V. Krivosheina, A. Dietz, O. Chkvorets, Phys. Lett. **B586**, 198-212 (2004). [hep-ph/0404088].
 - [33] S. Dodelson, A. Melchiorri, A. Slosar, Phys. Rev. Lett. **97**, 041301 (2006). [astro-ph/0511500].
 - [34] J. Hamann, S. Hannestad, G. G. Raffelt, I. Tamborra, Y. Y. Y. Wong, Phys. Rev. Lett. **105**, 181301 (2010). [arXiv:1006.5276 [hep-ph]].

- [35] J. Hamann, S. Hannestad, G. G. Raffelt, Y. Y. Y. Wong, JCAP **1109**, 034 (2011). [arXiv:1108.4136 [astro-ph.CO]].
- [36] P. Adamson *et al.* [MINOS Collaboration], Phys. Rev. Lett. **107**, 011802 (2011). [arXiv:1104.3922 [hep-ex]].
- [37] J. N. Abdurashitov *et al.* [SAGE Collaboration], Phys. Rev. C **80**, 015807 (2009).
- [38] F. Kaether, W. Hampel, G. Heusser, J. Kiko and T. Kirsten, Phys. Lett. B **685**, 47 (2010).
- [39] C. Giunti and M. Laveder, arXiv:1006.3244 [hep-ph].
- [40] J. M. Conrad, M. H. Shaevitz, [arXiv:1106.5552 [hep-ex]].
- [41] B. Armbruster *et al.* [KARMEN Collaboration], Phys. Rev. **D65**, 112001 (2002). [hep-ex/0203021].
- [42] P. Astier *et al.* [NOMAD Collaboration], Phys. Lett. **B570**, 19-31 (2003). [hep-ex/0306037].
- [43] Y. Declais *et al.*, Nucl. Phys. B **434**, 503 (1995); Y. Declais *et al.*, Phys. Lett. **B338**, 383 (1994).
- [44] F. Boehm, J. Busenitz, B. Cook, G. Gratta, H. Henrikson, J. Kornis, D. Lawrence, K. B. Lee *et al.*, Phys. Rev. **D64**, 112001 (2001). [hep-ex/0107009].
- [45] F. Dydak *et al.*, Phys. Lett. **B134**, 281 (1984).
- [46] A. Kuvshinnikov *et al.*, JETP Lett. 54, 253 (1991).
- [47] G. Vidyakin *et al.*, Sov. Phys. JETP 66, 243 (1987).
- [48] H. Kwon *et al.*, Phys. Rev. **D24**, 1097 (1981).
- [49] G. Zacek *et al.*, Phys. Rev. **D34**, 2621 (1986).
- [50] G. Karagiorgi, A. Aguilar-Arevalo, J. M. Conrad, M. H. Shaevitz, K. Whisnant, M. Sorel, V. Barger, Phys. Rev. **D75**, 013011 (2007). [hep-ph/0609177].
- [51] V. Barger, D. Marfatia and K. Whisnant, Phys. Rev. D **65**, 073023 (2002) [arXiv:hep-ph/0112119].
- [52] E. K. Akhmedov, R. Johansson, M. Lindner, T. Ohlsson, T. Schwetz, JHEP **0404**, 078 (2004). [hep-ph/0402175].
- [53] G. Karagiorgi, [arXiv:1110.3735 [hep-ph]].
- [54] G. S. Davies, f. t. N. Collaboration, [arXiv:1110.0112 [hep-ex]].
- [55] C. Giunti, Y. F. Li, Phys. Rev. **D80**, 113007 (2009). [arXiv:0910.5856 [hep-ph]].